

# Addressing the gas kinetics Boltzmann equation with branching paths statistics

Guillaume Terrée and Mouna El Hafi

*RAPSOSEE, UMR CNRS 5302, Mines Albi, Campus Jarlard; 81013 Albi CT cedex 09, France*

Stéphane Blanco and Richard Fournier

*LAPLACE, Université de Toulouse, CNRS, INPT, UPS, France*

Jérémie Dauchet

*Université Clermont Auvergne, CNRS, SIGMA Clermont,  
Institut Pascal, F-63000 Clermont-Ferrand, France*

Jacques Gautrais

*Centre de Recherches sur la Cognition Animale (CRCA),  
Centre de Biologie Intégrative (CBI), Université de Toulouse, CNRS, UPS;  
118 Route de Narbonne, Toulouse F-31062 cedex 4, France*

(Dated: August 17, 2018)

Several works have shown that it is possible to conceive non-linear Monte-Carlo algorithms, but these works have remained overlooked so far. It is commonly admitted that in non-linear physics it is necessary to start with a linearization step before then calling on the linear Monte-Carlo method. We show here how it is possible to avoid this linearization step in the particular case of the Boltzmann equation. Our method retains the exact character of the Monte-Carlo method (unbiased estimation with a reliable evaluation of its uncertainty). We also extend to non-linear transport a very strong property of Monte-Carlo algorithms in linear transport: the ability to perform probe calculus (evaluate a quantity at a given position and time without computing all the field at previous times). Another striking feature of this algorithm is its ability to focus on rare events, however scarce they may be, including very high energy events that are important from the applicative point of view.

**Keywords:** Monte Carlo method; branching random process; integral formulation; unbiased estimator; non-linear Boltzmann equation; gas kinetics

## I. INTRODUCTION

*In linear transport physics, and especially in radiative transfer physics [1, 2], the Monte-Carlo method (MCM) consists in simulating the history of numerous independent particles, from which mean observables can be deduced. Since its initial development, this numerical method has become extremely successful, because of its many qualities: a natural management of multi-dimensional phase space, a null systematic error compared to the mathematical and physical model, the confidence intervals given with the results, an ability to take into account numerous physical phenomena simultaneously, an efficient management of complex geometries, the ability to calculate sensitivities simultaneously, and easy parallelization [3, 4]. This success extends to all linear physics, not only to transport [5–7].*

*a. In non-linear physics, the Monte-Carlo method is commonly believed to be unusable:*

“So far as the author is aware, the extension of Monte Carlo methods to nonlinear processes has not yet been accomplished and may be impossible.” [8]

“Monte Carlo methods are not generally effective for nonlinear problems mainly because expectations are linear in character.” [9]

“A nonlinear problem must usually be linearized in order to use Monte Carlo technique.” [9]

However several examples lead us to moderate these assertions.

A first group of such examples is the lineage of the tests of Ermakov *et al* on the MCM used for solving non-linear kinetic equations [10]. At least twenty-five years ago, Gurov [11, 12] presented the calculation in the MCM of Fredholm integrals containing polynomial non-linearities, by branching estimation processes. Rasulov *et al* [13–15] showed how to use the MCM to resolve parabolic equations like the equation of heat, with a source term depending non-linearly on the density. Although barely cited or reused [16], these techniques were shown to work by their authors, who do not hide their intention to extend the MCM towards a broader class of non-linear problems.

A second group of examples [17] comes from the recent PhD works of J. Dauchet [18] and O. Farges [19], dedicated respectively to radiative transfer in photobioreactors and to the optimal design of concentrated solar power plants. The authors were confronted with numerical problems in which, on the one hand the geometrical complexity was so high that only statistical methods were looking affordable [20], and on the other hand nonlinearities were present – especially in the coupling law

between the local productivity inside the set-up and the radiative transfer. Dauchet has also tackled the problem of evaluating the radiative properties of microalgae by means of electromagnetics, accounting for their size and shape distribution [21]: here the non-linearity came from the fact that radiative properties are quadratic in the electric field amplitude, which he was basically able to calculate [22]. Confronted with these difficulties, J. Dauchet developed a technique to handle multi-folded integrals with one single stage of non-linearity in between [17], drawing his inspiration from Null Collision Algorithms (NCAs).

NCAs are the latest example we know of handling non-linearities in the MCM, although the example is drawn from linear transport – *eg* radiative transfer physics [23] and image synthesis [24, 25], semiconductor physics [26], neutronics [27–29], or even plasma physics [30]. These algorithms serve to account for the extinction properties of a medium, when they are highly variable. Their principle is to add virtual and ineffective colliders in order to make constant the total collision frequency. The NCAs are justified by the rigorous equivalence between the original and the modified transport problems; but they can also be viewed as a way to handle the non-linearity of the exponential Beer extinction law [31].

*b.* A *trick* shared in all these works is to convert the non-linearity into an increase in the dimension of the sampling space [17].

As a theoretical illustration, let us write that a searched quantity  $q$  is expressed as an expectation (either by mimicry of the physical process under study, or through a more mathematical reasoning) using the random variable (RV)  $\vec{X}$ , under the form:

$$q = E(a(\vec{X})h(\vec{X}) + b(\vec{X})) \quad (1a)$$

where  $E$  denotes the statistical expectation, and  $a$  and  $b$  are two deterministic functions. Suppose also that  $h(\vec{X})$  is only known as the expectation of an estimator  $\tilde{h}(\vec{X}; \vec{Y})$  using the sampling of a RV  $\vec{Y}$ :

$$q = E(a(\vec{X})E_{|\vec{X}}(\tilde{h}(\vec{X}; \vec{Y})) + b(\vec{X})) \quad (1b)$$

the subscript  $\bullet_{|\vec{X}}$  meaning that the value of  $\vec{X}$  is known. As the statistical expectation is linear and projective:

$$q = E(a(\vec{X})\tilde{h}(\vec{X}; \vec{Y}) + b(\vec{X})) \quad (1c)$$

It is thus useless to evaluate  $h(\vec{X})$  exactly (*ie* without statistical noise) at each value of  $\vec{X}$  in order to estimate  $q$  correctly (*ie* without bias, in MCM). Conversely, an algorithm estimating  $h(\vec{x})$  for any  $\vec{x}$  can be turned into an algorithm estimating  $q$ , simply by adding a first sampling of  $\vec{X}$ . This is one of the principal advantages of the Monte-Carlo method: its complexity increases linearly (and not exponentially) with the total dimension of the configuration space – here configurations are described

by the couple of RVs  $(\vec{X}; \vec{Y})$ . But this becomes false if the coupling law  $h \rightarrow q$  is non-linear. Imagine now that it is a square, then in a general manner

$$E(a(\vec{X})h(\vec{X})^2) \neq E(a(\vec{X})\tilde{h}(\vec{X}; \vec{Y})^2) \quad (2)$$

the same way as  $(u + v)^2 \neq u^2 + v^2$ .

However, in this quadratic case, we could replace  $\vec{Y}$  with two independent and identically distributed RVs,  $\vec{Y}_1$  and  $\vec{Y}_2$ , and then consider that:

$$E(a(\vec{X})h(\vec{X})^2) = E(a(\vec{X})\tilde{h}(\vec{X}; \vec{Y}_1)\tilde{h}(\vec{X}; \vec{Y}_2)) \quad (3)$$

The same technique is usable with monomial and polynomial functions, as:

$$\forall n \in \mathbb{N}, E(a(\vec{X})h(\vec{X})^n) = E(a(\vec{X})\prod_{i=1}^n \tilde{h}(\vec{X}; \vec{Y}_i)) \quad (4)$$

with the  $\vec{Y}_i$  all independent and identically distributed. This also extends to analytic functions, because in a Monte-Carlo calculation an infinite sum is no more than an integral.

*c. Despite the non-linearity of the gas kinetics Boltzmann equation,* the Monte-Carlo method has been commonly used to solve it. But the trick revealed in the previous paragraph has never been used, and the non-linearity has always been circumvented by using linearization techniques based on discretization of time and/or space. The numerical schemes obtained share the following operating principles: they build the story of a (big) swarm of statistically representative molecules, and because these cannot cross exactly, collisions are introduced using a proximity criterion [32–35]. There are a lot of variants being used today, depending on the collision quadrature used in time and space [36, 37], or on whether an Eulerian fluid model is used in tandem with the statistical model [38, 39]...

*d. The author's proposal is* to solve the Boltzmann equation with Monte-Carlo algorithms like those used in linear transport, without linearization or discretization, using the trick revealed in the previous paragraph along with the null collision technique. The trick alone will deal with the source term in the Boltzmann collision operator, and the null collisions are useful to handle the extinction term.

*e. What we have obtained* is a statistical numerical method in gas kinetics, the statistical formulations of which are given below. The method retains the advantages of the MCM from linear transport, its most striking properties being that:

- No mesh or time discretization is necessary in the method.
- The method enables probe calculus, *ie* it is possible to calculate the distribution function at a point of the phase space, without computing the rest of the field.

- Rarefaction of the gas at the probe does not compromise the relative precision of the calculations.
- Similarly, the frequency of rare events (in the space of speeds) can be estimated however scarce they may be.
- The method is limited in (spatial or temporal) Knudsen number; because it uses a branching estimation process, the mean complexity of which grows exponentially with the mean number of collisions.
- The branchings in the estimation process also create a variance problem, which is very sensitive to algorithmic choices. Today, a theoretical framework for understanding this is lacking.
- As a result of the two previous points, we are today essentially unable to perform a calculus on a steady state.

*f.* *This paper is organized as follows.* In section II, we show how to handle the non-linearity of the source term in the Boltzmann collision operator, in an academic case called the BKW mode [40] which has a symbolic expression. In section III, we shall see how to deal with extinction in the Boltzmann collision operator, in a very simplified toy model with a symbolic solution. In sections IV and V we deal with the full Boltzmann equation, firstly in a particular case [41] with a symbolic solution (and local equilibrium) and secondly in a more general case. We conclude in section VI.

## II. EXAMPLE: THE BKW MODE

*a.* *The Bobylev-Krook-Wu mode* was discovered simultaneously by these authors in 1976 [42, 43]. It is an explicit solution of the Boltzmann equation, associated with a particular set of physical conditions.

We place ourselves in ordinary 3-dimensional space [44]. The collision model consists of Maxwell molecules with isotropic scattering: the differential cross section  $\sigma_F$  is inversely proportional to the relative speed  $g$ , with no angular dependence. The gas is uniform, with a unit density and a peculiar velocity of zero. Thus  $f \equiv f(\vec{c}; t)$ , and with the adequate non-dimensionalization of time the Boltzmann equation reads:

$$\partial_t f(\vec{c}; t) = -f(\vec{c}; t) + \int_{E_c} d\vec{c}_* \int_{E_u} \frac{d\vec{u}'}{4\pi} f(\vec{c}'; t) f(\vec{c}'_*; t) \quad (5)$$

where  $E_c$  and  $E_u$  denote respectively the spaces of velocities and directions (so  $E_u$  is the unit sphere of  $E_c$ ), and  $\vec{c}'$  and  $\vec{c}'_*$  state

$$\begin{cases} \vec{c}' = \frac{1}{2}(\vec{c} + \vec{c}_* + g\vec{u}') \\ \vec{c}'_* = \frac{1}{2}(\vec{c} + \vec{c}_* - g\vec{u}') \\ g = \|\vec{c} - \vec{c}_*\| \end{cases} \quad (6)$$

In this case, the Boltzmann equation admits the particular solution known as BKW mode

$$f(\vec{c}; t) = \frac{\exp(-\vec{c}^2/(2Kc_q^2))}{2(\sqrt{2\pi K}c_q)^3} \left( \frac{5K-3}{K} + \frac{1-K}{K^2} \times \frac{\vec{c}^2}{c_q^2} \right) \quad (7a)$$

with

$$K = 1 - \frac{2}{5} \exp(-t/6) \quad (7b)$$

and  $c_q$  the Root Mean Square velocity on each axis (RMS velocity). With the  $\frac{2}{5}$  factor in the expression of  $K$ ,  $f$  is definite and positive for  $t \geq 0$ . Fig. 1 gives a graphical overview of the BKW mode.

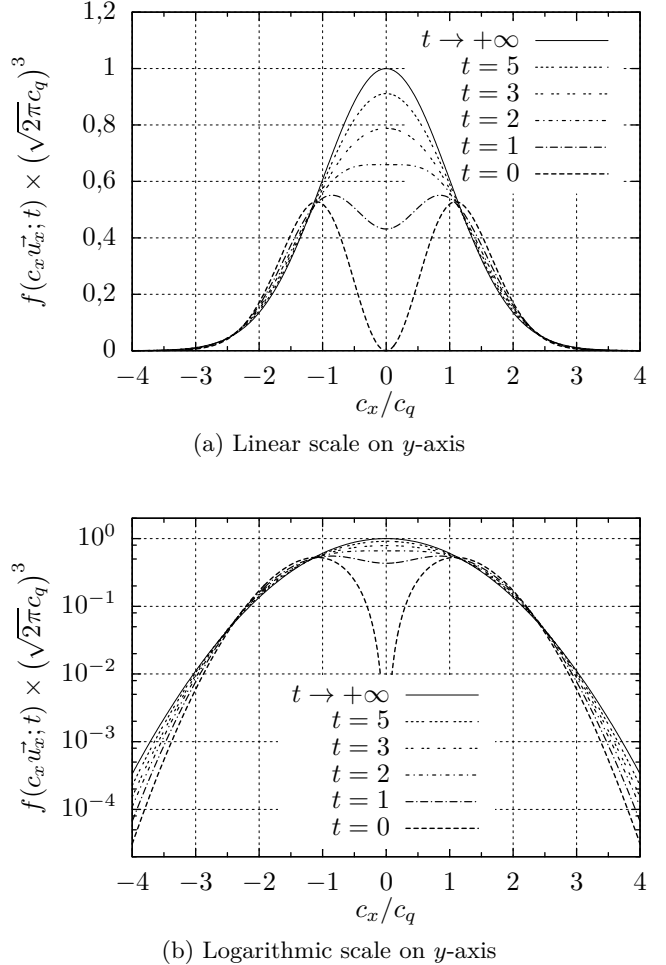


FIG. 1. The distribution function  $f$  along the  $(Ox)$  axis of the velocity space, according to the BKW mode described in Eq. (7), at several times  $t$ .  $\vec{u}_x$  denotes the  $x$  unit vector.

*b.* *In order to build a Monte-Carlo calculation* in the physical situation of the BKW mode, let us rewrite the evolution Eq. (5).

$$\partial_t f(\vec{c}; t) = -f(\vec{c}; t) + s_{is}(\vec{c}; t) \quad (8a)$$

with

$$s_{is}(\vec{c}; t) = \int_{E_c} d\vec{c}_* \int_{E_u} \frac{d\vec{u}'}{4\pi} f(\vec{c}'; t) f(\vec{c}'_*; t) \quad (8b)$$

If it is assumed that the initial condition is “ $f$  is known at  $t = 0$ ”, the time-differential Eq. (8a) can be formally solved, giving:

$$\forall t \geq 0, f(\vec{c}; t) = \int_{-\infty}^t dt' \exp(-(t - t')) \times \\ \left( H(t') s_{is}(\vec{c}; t') + H(-t') f(\vec{c}; 0) \right) \quad (9)$$

where  $H$  is the Heaviside step function:  $H(t) = 1$  if  $t > 0$ ,  $H(t) = 0$  if  $t < 0$ .

Together, Eqs. (9) and (8b) give a second kind Fredholm writing of  $f$ . By choosing probability densities in order to sample  $t'$ ,  $\vec{c}_*$ , and  $\vec{u}'$ , this can be converted into the Monte-Carlo algorithm 1, intended to estimate  $f(\vec{c}; t)$  with  $(\vec{c}; t) \in E_c \times \mathbb{R}^+$ . Because algorithm 1 is recursive, its ability to complete will be known when setting how  $t'$ ,  $\vec{c}_*$ , and  $\vec{u}'$  are sampled.

```

Input: A point  $(\vec{c}; t)$  in  $E_c \times \mathbb{R}^+$ 
Output: A point estimate of  $f(\vec{c}; t)$ 
Sample  $T'$  in  $(-\infty; t]$ :  $t'$  is obtained;
if  $t' \leq 0$  then
  return  $\frac{\exp(-(t - t')) f(\vec{c}; 0)}{p_{T'}(t')}$ ; //  $f(\vec{c}; 0)$  is known
else
  Sample  $\vec{C}_*$ :  $\vec{c}_*$  is obtained;
  Sample  $\vec{U}'$ :  $\vec{u}'$  is obtained;
   $\vec{c}' \leftarrow \frac{1}{2}(\vec{c} + \vec{c}_* + \|\vec{c} - \vec{c}_*\| \vec{u}');$ 
   $\vec{c}'_* \leftarrow \frac{1}{2}(\vec{c} + \vec{c}_* - \|\vec{c} - \vec{c}_*\| \vec{u}');$ 
  Estimate  $f(\vec{c}'; t')$  using this algorithm:  $\tilde{f}_1(\vec{c}'; t')$  is
  obtained;
  Estimate  $f(\vec{c}'_*; t')$  using this algorithm:  $\tilde{f}_2(\vec{c}'_*; t')$  is
  obtained; // independently to  $\tilde{f}_1(\vec{c}'; t')$ 
  return  $\frac{\exp(-(t - t')) \tilde{f}_1(\vec{c}'; t') \tilde{f}_2(\vec{c}'_*; t')}{4\pi p_{T'}(t') p_{\vec{C}_*}(\vec{c}_*) p_{\vec{U}'}(\vec{u}')};$ 

```

**Algorithm 1:** Algorithm for estimating  $f(\vec{c}; t)$ , valid in the conditions of the BKW mode described in section II (uniform and unit density, Maxwell molecules...)

c. The recursive character of algorithm 1 is a feature common to all Monte-Carlo algorithms based on second kind Fredholm formulations. It is found in all multiple scattering problems of transport physics. But contrary to what happens in linear transport, each recursive stage of an estimation of  $f$  by algorithm 1 is likely to call itself *more than once*. So, to be exact, the estimation process no longer consists in following a (virtual) particle path, but rather in following a particle *tree*.

We began the formal development of our proposal with a recursive integral formulation, rather than with a path integral. We will continue in this way, and invoke the notion of path (or tree) as little as possible. However, for the sake of understanding, it seems useful to illustrate here what the branching estimation paths will look like.

At the same time, we propose a way to locate in such estimation trees. We take our inspiration from a previous proposal of Gurov [11, 12, 45]. Any intermediate estimate of  $f$  in a estimation tree is indexed with an integer sequence, according to the following rules:

- Only the sequences  $\mathbb{N}^* \rightarrow \mathbb{N}$ , stationary at 0, in which all terms are null since the first null term, are used.
- The degree of the sequence (the index of its furthest non-zero term) indicates the depth of the estimate inside the estimation tree; *ie* the number of  $(T'; \vec{C}_*; \vec{U}')$  samplings which lead to the point where the considered intermediary estimate is needed.
- Thus, the final estimate given by the first call of algorithm 1 is indexed by the null sequence.
- Among the non-zero terms, the  $i^o$  term equals 1 if at the  $i^o$  depth of recursion the branch of estimating  $\vec{c}'$  has been followed, while it equals 2 if the branch of estimating  $\vec{c}'_*$  has been followed.

An example of an estimation tree, with this location indexing, is given in Fig. 2.

d. We propose the following choice for sampling  $t'$ ,  $\vec{c}_*$ , and  $\vec{u}'$ :

$$\left\{ \begin{array}{l} p_{T'} : \left\{ \begin{array}{l} (-\infty; t] \rightarrow \mathbb{R}^+ \\ t' \mapsto \exp(-(t - t')) \end{array} \right. \\ p_{\vec{C}_*} : \left\{ \begin{array}{l} E_c \rightarrow \mathbb{R}^+ \\ \vec{c}_* \mapsto (\sqrt{2\pi} c_q)^{-3} \exp(-\vec{c}_*^2/(2 c_q^2)) \end{array} \right. \\ p_{\vec{U}'} : \left\{ \begin{array}{l} E_u \rightarrow \mathbb{R}^+ \\ \vec{u}' \mapsto (4\pi)^{-1} \end{array} \right. \end{array} \right. \quad (10)$$

$T'$  follows a unit exponential law to the left of  $t$ ,  $\vec{C}_*$  has a Maxwellian distribution with null peculiar velocity and  $c_q$  RMS speed, and  $\vec{U}'$  is isotropically distributed. Algorithm 1 with these probability densities will be named hereafter algorithm 2: it is displayed in a separate figure.

This choice, although guided by a desire for simplicity, brings two interesting qualities to algorithm 1 (now 2):

1. The expectation of the recursion, defined as the number of  $T'$  samplings per final estimation (*ie* the number of lines in an estimation tree), is finite. This implies that algorithm 2 surely completes.
2. If at  $t = 0$  the distribution  $f$  is at equilibrium:

$$f(\vec{c}; t = 0) = \frac{\exp(-\vec{c}^2/(2 c_q^2))}{(\sqrt{2\pi} c_q)^3} \quad (11)$$

then algorithm 2 has a null variance.

*Principle of proof (1<sup>st</sup> point).* Let us consider the expectation of the recursion of algorithm 2 starting at  $(\vec{c}; t)$ ,

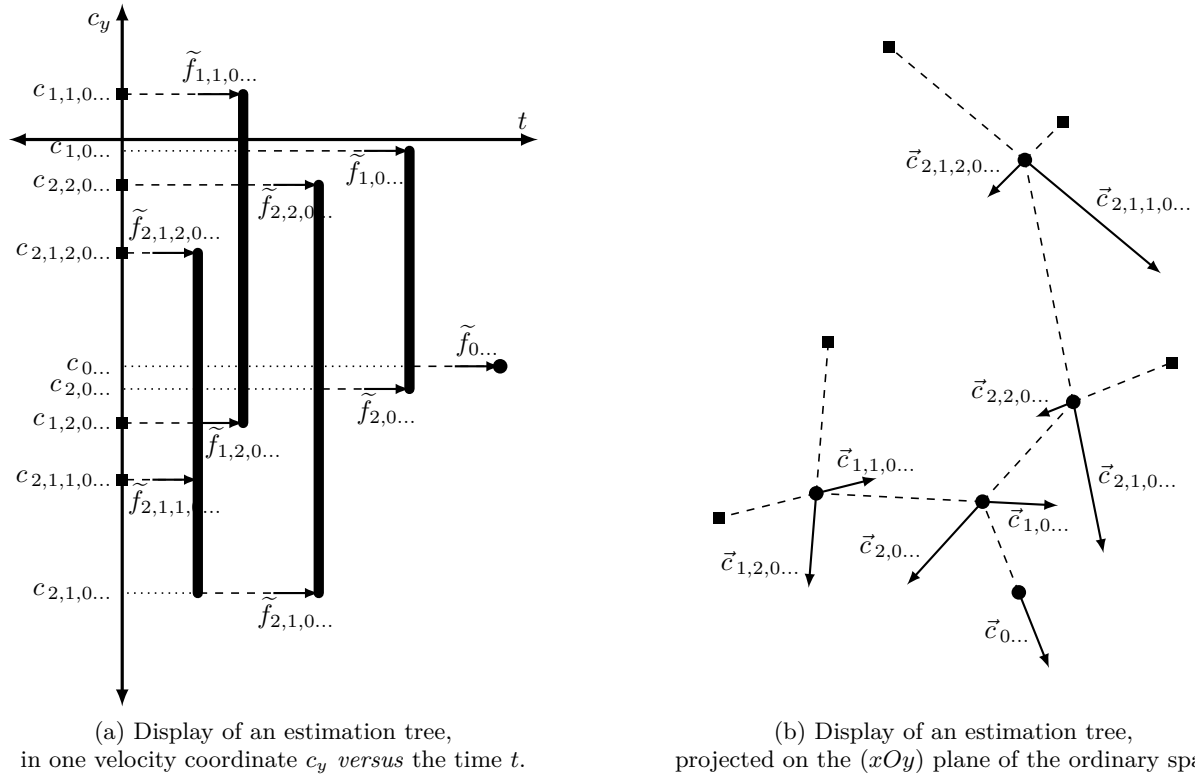


FIG. 2. Illustration of an estimation tree as generated by algorithm 1, with locations indexed as proposed in paragraph II 0 c. The same tree is displayed, in (a) with one velocity coordinate *versus* time, in (b) with 2 ordinary space coordinates. For the sake of readability, the speeds have been indexed identically to the estimations that are made there. The collision locations are denoted in (b) by circles and in (a) by rounded cap vertical lines. Squares denote where the tree meets the initial condition.

```

Input: A point  $(\vec{c}; t)$  in  $E_c \times \mathbb{R}^+$ 
Output: A point estimate of  $f(\vec{c}; t)$ 

Sample  $T'$  following a unit exponential law to the left of
 $t$ :  $t'$  is obtained;
if  $t' \leq 0$  then return  $f(\vec{c}; 0)$ ; //  $f(\vec{c}; 0)$  is known
else
  Sample  $\vec{C}_*$  following a Maxwellian distribution, with
  null peculiar velocity and  $c_q$  RMS speed:  $\vec{c}_*$  is
  obtained;
  Sample  $\vec{U}'$  isotropically:  $\vec{u}'$  is obtained;
   $\vec{c}' \leftarrow \frac{1}{2}(\vec{c} + \vec{c}_* + \|\vec{c} - \vec{c}_*\| \vec{u}');$ 
   $\vec{c}'_* \leftarrow \frac{1}{2}(\vec{c} + \vec{c}_* - \|\vec{c} - \vec{c}_*\| \vec{u}');$ 
  Estimate  $f(\vec{c}'; t')$  using this algorithm:  $\tilde{f}_1(\vec{c}'; t')$  is
  obtained;
  Estimate  $f(\vec{c}_*'; t')$  using this algorithm:  $\tilde{f}_2(\vec{c}_*'; t')$  is
  obtained; // independently of  $\tilde{f}_1(\vec{c}'; t')$ 
return  $(\sqrt{2\pi c_q})^3 \exp(-\vec{c}_*'^2/(2c_q^2)) \tilde{f}_1(\vec{c}'; t') \tilde{f}_2(\vec{c}_*'; t')$ 

```

**Algorithm 2:** Algorithm for estimating  $f(\vec{c}; t)$ , valid in the conditions of the BKW mode described in section II (uniform and unit density, Maxwell molecules...). The sampling choices listed in Eq. (10) are used.

defined as the expectation of the number of times  $T'$  ran-

dom variables will be sampled. This defines a function  $rec : E_c \times \mathbb{R}^+ \rightarrow [1; +\infty]$ .

Reading algorithm 1, an integral equation on  $rec$  can be obtained (as for the calculated quantity  $f$ ). It reads:

$$rec(\vec{c}; t) = \int_{-\infty}^t p_{T'}(t') dt' \left( 1 + H(-t') \times 0 + H(t') \int_{E_c} p_{\vec{C}_*}(\vec{c}_*) d\vec{c}_* \int_{E_u} p_{\vec{U}'}(\vec{u}') d\vec{u}' \times (rec(\vec{c}'; t') + rec(\vec{c}_*'; t')) \right) \quad (12)$$

Then the sampling choices we have made in Eqs. (10) are entered, which gives:

$$rec(\vec{c}; t) = \int_{-\infty}^t \exp(-(t - t')) dt' \left( 1 + H(t') \int_{E_c} \frac{\exp(-\vec{c}_*'^2/(2c_q^2)) d\vec{c}_*}{(\sqrt{2\pi c_q})^3} \int_{E_u} \frac{d\vec{u}'}{4\pi} \times (rec(\vec{c}'; t') + rec(\vec{c}_*'; t')) \right) \quad (13)$$

In order to solve this second kind Fredholm expression manually, it can be derived with respect to  $t$ , which gives

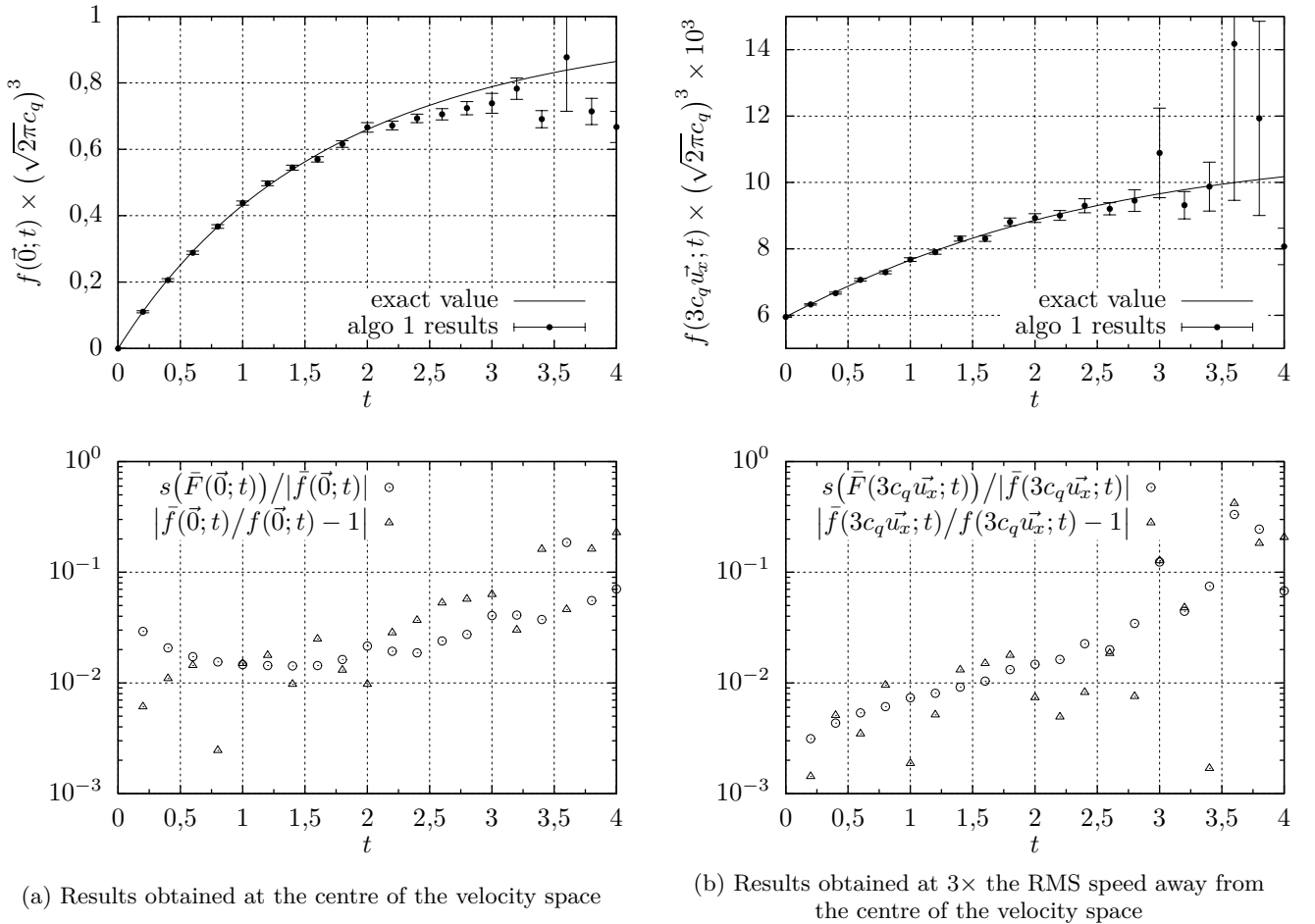


FIG. 3. Results obtained by algorithm 2, applied to the BKW mode described in Eq. (7). Two probe points in the velocity space are considered, where we follow the distribution function  $f$  along the time  $t$ . The graphs at the top give a graphical comparison between the results (given with confidence intervals of 1 standard deviation) and the expected values. The graphs at the bottom show, with the same results, the relative standard deviation (circles) (given by the calculations) beside the error actually made (triangles). Each displayed point was obtained through running  $10^4$  realizations of algorithm 2.

a differential system on  $rec$ :

$$\left\{ \begin{array}{l} \partial_t rec(\vec{c}; t) = -rec(\vec{c}; t) + 1 + \\ \forall t \geq 0, \left\{ \int_{E_c} \frac{\exp(-\vec{c}_*^2/(2c_q^2)) d\vec{c}_*}{(\sqrt{2\pi c_q})^3} \int_{E_u} \frac{d\vec{u}'}{4\pi} \times \right. \\ \left. (rec(\vec{c}'; t) + rec(\vec{c}'_*; t)) \right) \\ rec(\vec{c}; t = 0) = 1 \end{array} \right. \quad (14)$$

$rec$  is uniform at  $t = 0$ , and its derivative preserves this uniformity: so here  $rec(\vec{c}; t) \equiv rec(t)$ . Finally the system is easily solved in:

$$rec(\vec{c}; t) = 2 \exp(t) - 1 \quad (15)$$

which is finite for all  $(\vec{c}; t) \in E_c \times \mathbb{R}^+$ .  $\square$

*Principle of proof (2<sup>nd</sup> point).* We call  $\tilde{F}(\vec{c}; t)$  an estimator of  $f(\vec{c}; t)$ , obtained through algorithm 2. We assume

that the initial distribution  $f(\vec{c}; t = 0)$  is the equilibrium distribution described in Eq. (11).

Now consider the following induction hypothesis, to be applied anywhere in an estimation tree:  $\tilde{F}(\vec{c}; t) = (\sqrt{2\pi c_q})^{-3} \exp(-\vec{c}^2/(2c_q^2))$ , ie  $f$  is always estimated as the equilibrium distribution with no variance.

Starting algorithm 2 there are two possibilities:  $T' \leq 0$  and we are at a leaf of the tree, or  $T' > 0$  and we are at a non-leaf node of the tree.

If  $T' \leq 0$  then:

$$\begin{aligned} \tilde{F}(\vec{c}; t) &= f(\vec{c}; 0) \\ &= \frac{\exp(-\vec{c}^2/(2c_q^2))}{(\sqrt{2\pi c_q})^3} \end{aligned} \quad (16)$$

the induction hypothesis is valid.

If  $T' > 0$  then:

$$\tilde{F}(\vec{c}; t) = \frac{(\sqrt{2\pi c_q})^3 \tilde{F}_1(\vec{C}'; T') \tilde{F}_2(\vec{C}'_*; T')}{\exp(-\vec{C}'^2/(2c_q^2))}$$

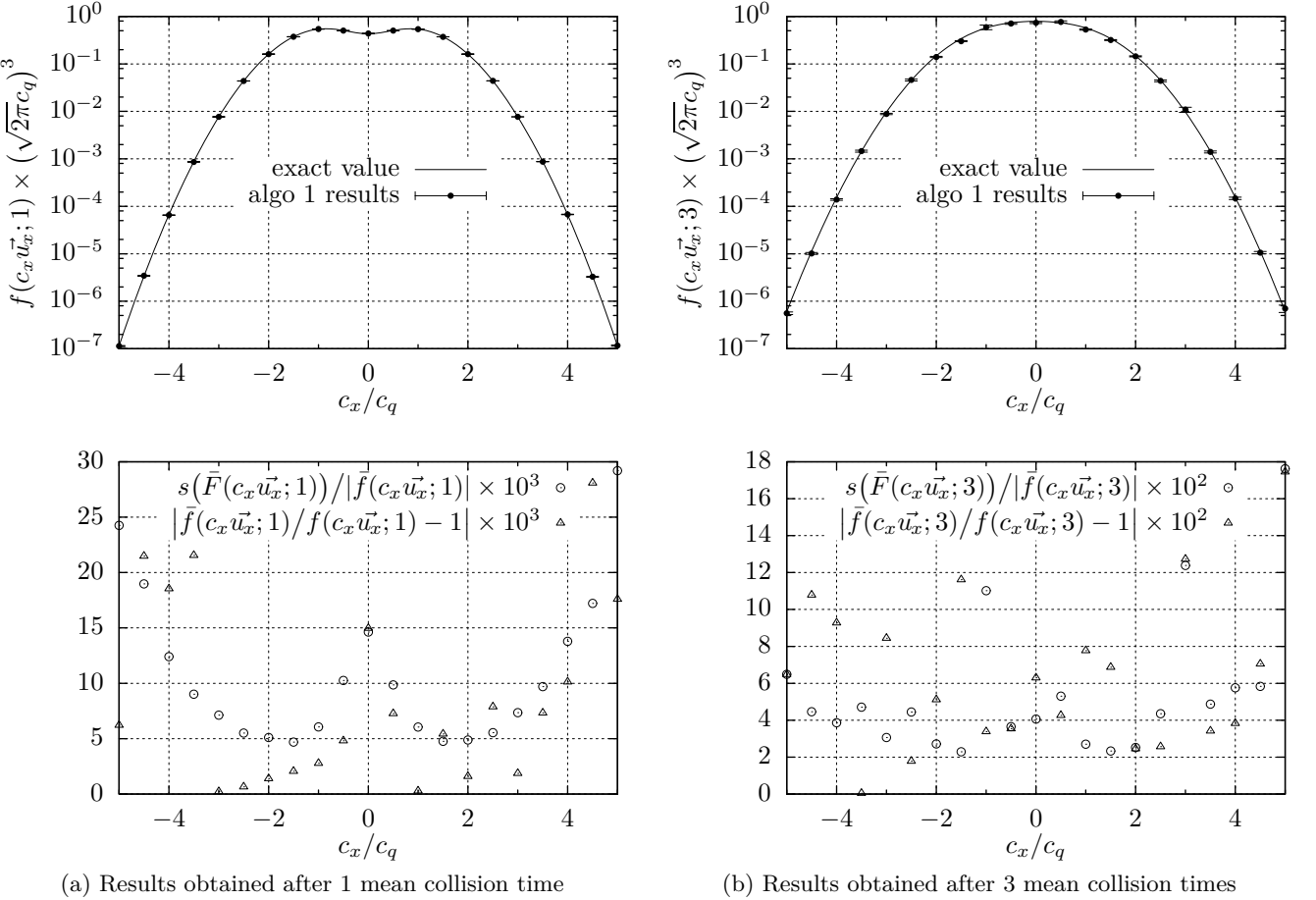


FIG. 4. Results obtained by algorithm 2, applied to the BKW mode described in Eq. (7). The probe points are spread on the ( $Ox$ ) axis of the velocity space, and only two dates are considered. The graphs at the top give a graphical comparison between the results (given with confidence intervals of 1 standard deviation) and the expected values. The graphs at the bottom show, with the same results, the relative standard deviation (circles) (given by the calculations) beside the error actually made (triangles). Each displayed point was obtained through running  $10^4$  realizations of algorithm 2.

where  $\vec{C}'$  and  $\vec{C}'_*$  are the random variables (RVs) corresponding to the values  $\vec{c}'$  and  $\vec{c}'_*$  in algorithm 2. If the induction hypothesis holds for  $\tilde{F}_1(\vec{C}'; T')$  and  $\tilde{F}_2(\vec{C}'_*; T')$ , then:

$$\begin{aligned} \tilde{F}(\vec{c}; t) &= \frac{\exp(-\vec{C}'^2/(2c_q^2)) \exp(-\vec{C}'_*^2/(2c_q^2))}{(\sqrt{2\pi}c_q)^3 \exp(-\vec{C}^2/(2c_q^2))} \\ &= \frac{\exp(-\vec{c}^2/(2c_q^2))}{(\sqrt{2\pi}c_q)^3} \end{aligned} \quad (17)$$

because  $\vec{C}'^2 + \vec{C}'_*^2 = \vec{c}^2 + \vec{C}^2$ .

The induction hypothesis applies in this case also.

Because the estimation tree is finite (see the previous point), the induction hypothesis applies from the leaves of the tree to any node of the tree, root included.  $\square$

e. *Numerical experiments* were carried out in which algorithm 2 was operated to calculate  $f$  at several points of the phase spacetime. The physical situation considered is the BKW situation expressed in Eq. (7), ie the initial

distribution is at maximal disequilibrium:

$$f(\vec{c}; 0) = \frac{5\vec{c}^2}{9c_q^2} \left( \sqrt{\frac{6\pi}{5}} c_q \right)^{-3} \exp\left(-\vec{c}^2 \left/ \left( \frac{6}{5} c_q^2 \right) \right.\right) \quad (18)$$

For each point where  $f$  was calculated,  $10^4$  realizations were used. The results are displayed in Figs. 3 and 4.

A first feature of the performance of algorithm 2 is that the variance of its result increases with the time elapsed since the initial condition. This is logical. When the elapsed time increases, on average the estimation trees are padded. Because the relation between the result and the equilibrium value is exactly the product of these relations at every leaf of the estimation tree (this can be understood through the 2<sup>nd</sup> proof just above), more leaves means more variance in the final result. Otherwise, the modelling process we applied to the mean recursion  $rec(\vec{c}; t)$  through Eqs. (12) to (14) can be applied to the estimator variance – this will be the subject of a future paper –, which does indeed show that this variance increases with the time  $t$ .

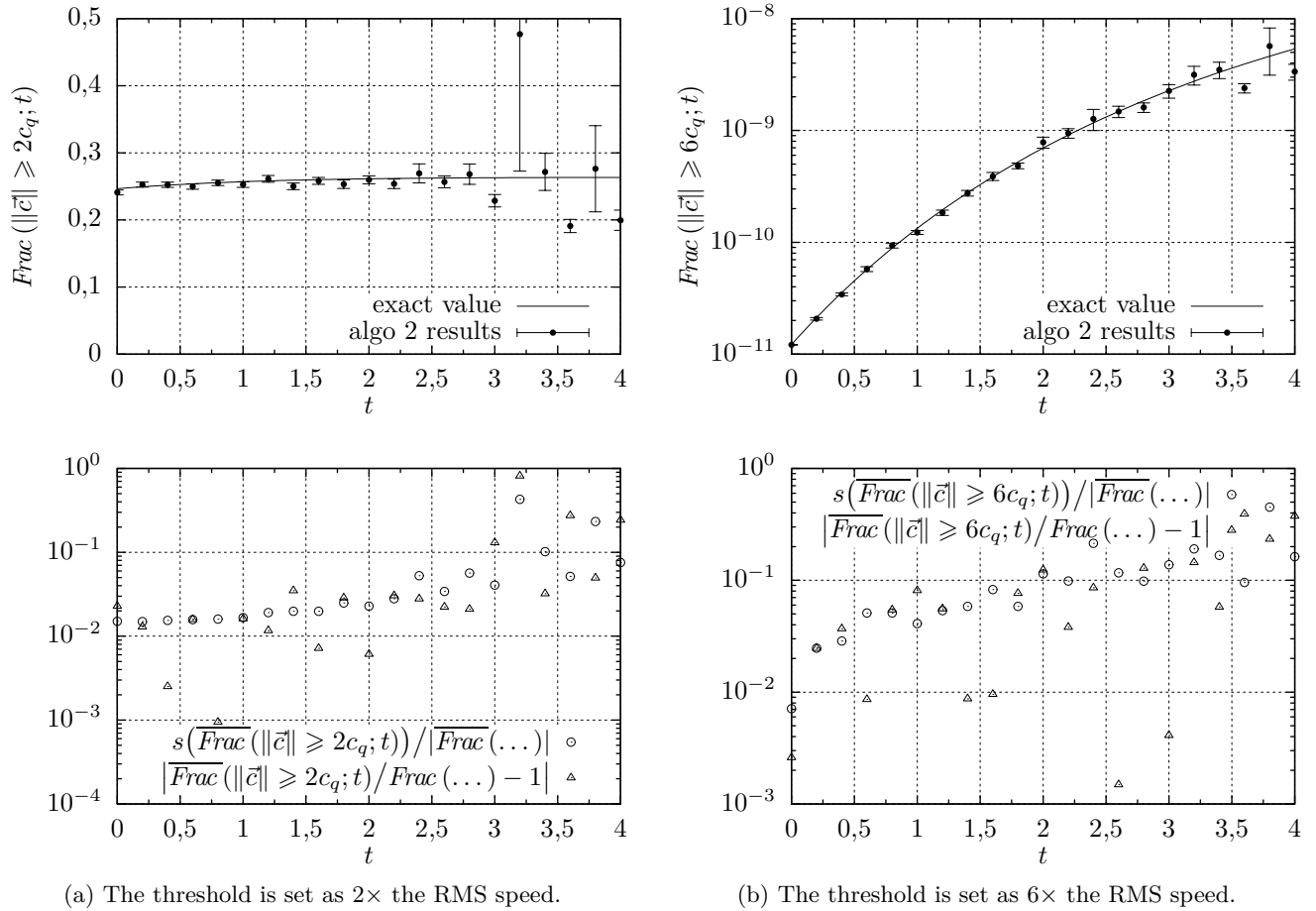


FIG. 5. Results obtained by algorithm 3 combined with the sampling laws listed in Eqs. (10) and (19), and applied to the BKW mode described in Eq. (7). Two constant speeds are considered: along the time  $t$ , we follow how many particles have a speed above these thresholds. The graphs at the top give a graphical comparison between the results (given with confidence intervals of 1 standard deviation) and the expected values. The graphs at the bottom show, with the same results, the relative standard deviation (circles) (given by the calculations) beside the error actually made (triangles). Each displayed point was obtained through running  $10^4$  realizations of algorithm 3.

**Input:** A speed  $c_0$  and a time  $t$   
**Output:** A point estimate of  $\text{Frac}(\|\vec{c}\| \geq c_0; t)$ , the fraction of particles of which speed exceeds  $c_0$  at time  $t$

Sample  $C_f$ :  $c_f$  is obtained;  $\quad // \quad c_f \geq c_0$   
 Sample  $\vec{U}_f$ :  $\vec{u}_f$  is obtained;  
 Estimate  $f(c_f \vec{u}_f; t)$  using algorithm 1:  $\tilde{f}(c_f \vec{u}_f; t)$  is obtained;  
 return  $\frac{c_f^2 \tilde{f}(c_f \vec{u}_f; t)}{p_{C_f}(c_f) p_{\vec{U}_f}(\vec{u}_f)}$ ;

**Algorithm 3:** Algorithm for estimating fractions of particles with high kinetic energy, valid in the conditions of the BKW mode described in section II (uniform and unit density, Maxwell molecules...)

A more interesting behaviour of algorithm 2 is that the variance of its result depends very little on the position in the phase space. In particular, it is nearly independent of

the rarefaction: in Fig. 4, we see that when  $f$  is divided by  $10^6$  while placing in the velocity space, the relative error increases only by a factor of 5.

In order to verify this last feature in more depth, we decided to compute high-energy fractions of the gas. The quantity we calculated was  $\text{Frac}(\|\vec{c}\| \geq c_0; t)$ , the fraction of molecules of which the total speed exceeds a given threshold  $c_0$  at time  $t$ . It is a direct integral of  $f$  on  $E_c$ : we computed it using algorithm 2, with the additional initial sampling of a RV  $\vec{C}_f = C_f \vec{U}_f$ . Algorithm 3 explains this; the added sampling law is:

$$\begin{cases} p_{C_f}(c_f) = \frac{c_0 \left( \left( \frac{c_0}{c_q} \right)^2 - 2 \right)}{\left( \left( \frac{c_0}{c_q} \right)^2 - 2 \right) (c_f - c_0) + c_0} & \text{if } c_0 > 2c_q \\ p_{C_f}(c_f) = \frac{2c_q}{(2c_q + c_f - c_0)^2} & \text{if } c_0 \leq 2c_q \\ p_{\vec{U}_f}(\vec{u}_f) = (4\pi)^{-1} & \end{cases} \quad (19)$$

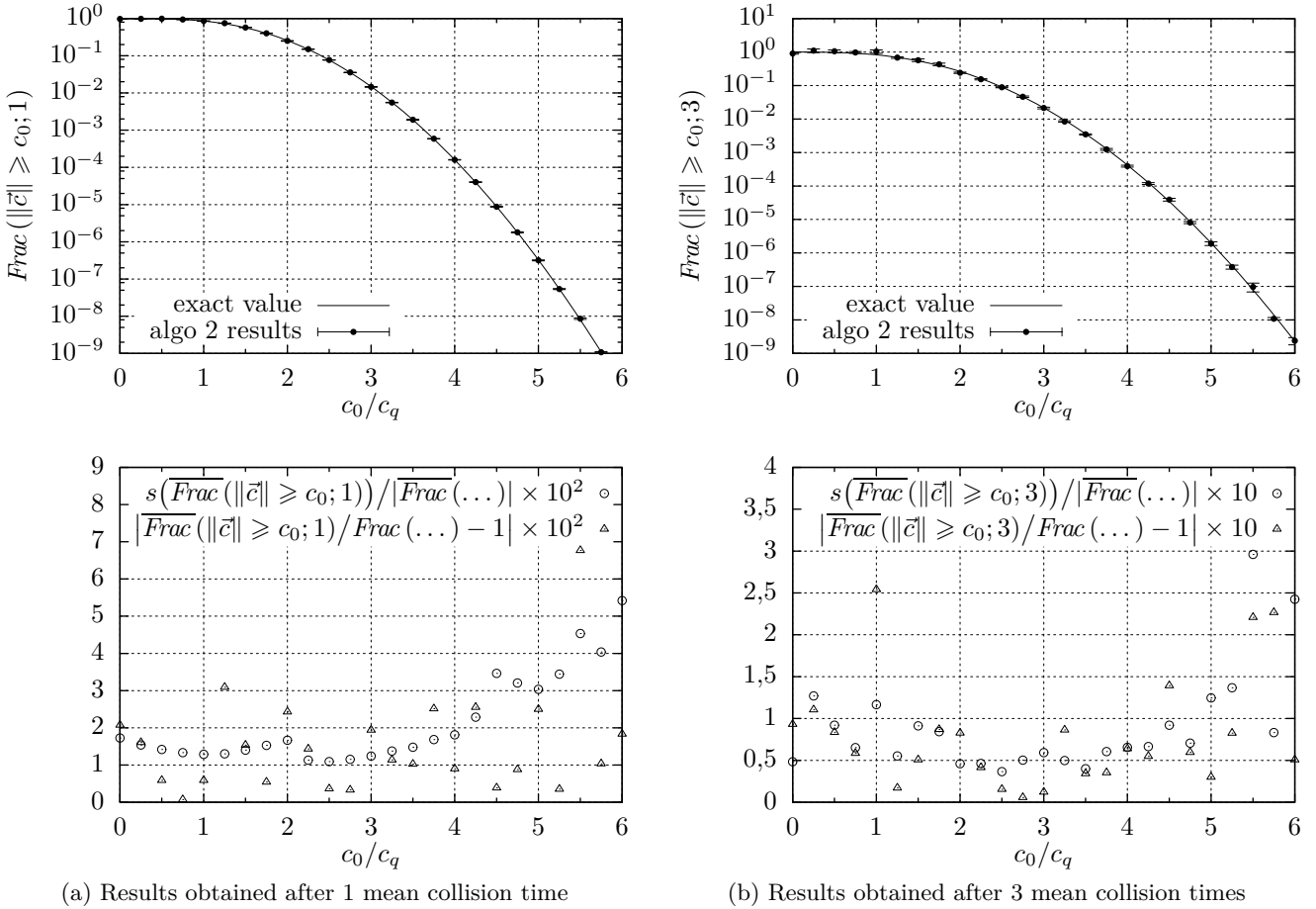


FIG. 6. Results obtained by algorithm 3 combined with the sampling laws listed in Eqs. (10) and (19), and applied to the BKW mode described in Eq. (7). We calculate the distribution of particles along the speed  $\|\vec{c}\|$ , *i.e.* how many particles have a speed above any given threshold  $c_0$ ; only two dates are considered. The graphs at the top give a graphical comparison between the results (given with confidence intervals of 1 standard deviation) and the expected values. The graphs at the bottom show, with the same results, the relative standard deviation (circles) (given by the calculations) beside the error actually made (triangles). Each displayed point was obtained through running  $10^4$  realizations of algorithm 3.

The results of algorithms 3 and 2, with sampling laws listed in Eqs. (19) and (10), are displayed in Figs. 5 and 6. There seems to be no problem in quantifying tiny parts of the gas, especially those located at high kinetic energy, even fractions as small as one billionth of the total.

### III. TOY MODEL, WITH NULL COLLISIONS

*a.* *In the previous section,* we used the BKW mode as an example of gas kinetics. This theoretical case is built on a very particular combination: the uniform density and the Maxwell collision model together make the collision frequency constant, in the whole phase space. Thus the extinction in the Boltzmann dynamics becomes artificially linear. We have written  $f(\vec{c}; t)$  as a sum of contributions of the source term due to inward collisions, weighted with the Beer extinction law, in Eq. (9). This is in fact always feasible, but there the exponential of the Beer law uses the time only multiplied with a constant

coefficient (which can be set to unity thanks to proper non-dimensionalizing, as was done in this case), which is very convenient for sampling. In a more general case, the collision frequency depends on  $f$ , which introduces through the exponential term in Eq. (9) an additional non-linearity to the one contained in the source term.

We show hereafter how to deal with the non-linearity of the extinction, in the Boltzmann equation. This is done on a very simplified case, built as the extinction of the Boltzmann dynamics isolated without source term or phase space. It is only the quadratic ordinary differential system, here written in  $f(t)$ :

$$\begin{cases} f'(t) = -\alpha f(t)^2 \\ f(0) = f_0 \end{cases} \quad (20)$$

where  $\alpha$  and  $f_0$  are arbitrary positive constants. It admits on  $\mathbb{R}^+$  the single solution:

$$f(t) = \frac{f_0}{\alpha f_0 t + 1} \quad (21)$$

b. A way to solve Eq. (20) numerically, with the Monte-Carlo method, would be to use a linear solution of Eq. (20), as we did in the previous section in Eq. (9). Indeed here:

$$f'(t) = -(\alpha f(t)) \times f(t) \quad (22)$$

and so

$$\forall t \geq 0, f(t) = \int_{-\infty}^t dt' \alpha \check{f}(t') \exp\left(-\alpha \int_{t'}^t dt'' \check{f}(t'')\right) \times \left(H(t') \times 0 + H(-t') f_0\right) \quad (23)$$

where

$$\check{f}(t) = H(t) f(t) + H(-t) f_0 \quad (24)$$

Combined with the use of independent and identically distributed RVs applied to a Taylor series of the exponential function, as proposed in section I 0 b and detailed in [18], Eq. (23) leads to a recursive integral writing of  $f(t)$ , which can be turned into a Monte-Carlo algorithm. However, this is not what we are going to use.

c. The technique we rely on is called, among other names, a Null Collision Algorithm (NCA) [46]. On the examples in this paper, it will remove the need for a Taylor series. In fact, NCAs are formally equivalent to the use of a Taylor series of the exponential extinction law, which we mentioned just above; this has been explained for example in [31]. But the way the NCAs are built relates to a physical interpretation, and their convergence is very simple to obtain, which is why we have chosen this approach.

The principle of a NCA is to introduce an arbitrary collision frequency, here noted  $\hat{\nu}$ . We thus transform the Eq. (20) in:

$$f'(t) = -\hat{\nu} f(t) + (\hat{\nu} f(t) - \alpha f(t)^2) \quad (25)$$

Considering  $-\hat{\nu} f(t)$  as an extinction and  $(\hat{\nu} f(t) - \alpha f(t)^2)$  as a source term, we now express:

$$\forall t \geq 0, f(t) = \int_{-\infty}^t dt' \hat{\nu} \exp(-\hat{\nu}(t - t')) \times \left(H(t') \left(f(t) - \frac{\alpha f(t)^2}{\hat{\nu}}\right) + H(-t') f_0\right) \quad (26)$$

This is where the name “Null Collision Algorithm” comes from. The extinction frequency is set to an arbitrary value  $\hat{\nu}$ . This is compensated by adding a source term of particles having encountered null collisions – collisions without effect. Thus the transport problem remains the same, only the algorithmic is modified.

In the following we call  $\hat{\nu}$  the “raised collision frequency”. This name arises from the fact that in early implementations of NCAs [26, 30, 47],  $\hat{\nu}$  was actually having to exceed the real extinction frequency everywhere for the algorithms to work. It has been demonstrated recently that this constraint is generally not mandatory [23] (but  $\hat{\nu}$  has, however, to be positive); nevertheless, complying with it improves the convergence in most cases.

d. By setting a probability density for the integration variable  $t'$  in Eq. (26) at every  $t \geq 0$ , we obtain a recursive Monte-Carlo algorithm for evaluating  $f(t)$ . We choose this density arbitrary as the exponential term in Eq. (26):

$$p_{T'} : \begin{cases} (-\infty; t] \rightarrow \mathbb{R}^{+*} \\ t' \mapsto \hat{\nu} \exp(-\hat{\nu}(t - t')) \end{cases} \quad (27)$$

for the sake of simplicity, and this choice will appear reasonable through the section. The result is algorithm 4.

**Input:** A time  $t \geq 0$   
**Output:** A point estimate of  $f(t)$

Sample  $T'$  following an exponential law to the left of  $t$ , with constant  $\hat{\nu}$ :  $t'$  is obtained;  
**if**  $t' \leq 0$  **then return**  $f_0$ ;  
**else**  
    Estimate  $f(t')$  using this algorithm:  $\tilde{f}_1(t')$  is obtained;  
    Estimate at new  $f(t')$  using this algorithm:  $\tilde{f}_2(t')$  is obtained; // independently of  $\tilde{f}_1(t')$   
    **return**  $\tilde{f}_1(t') \left(1 - \frac{\alpha \tilde{f}_2(t')}{\hat{\nu}}\right)$ ;

**Algorithm 4:** Algorithm for estimating  $f(t)$ , as described in Eq. (20)

In the same way as shown in the previous section, we can prove that the expected recursion of algorithm 4, starting at any arbitrary time, is finite. Defining the recursion  $rec$  as the total number of  $T'$  sampling – as in the previous section – we obtain a very similar result:

$$rec(t) = 2 \exp(\hat{\nu}t) - 1 \quad (28)$$

The same modelling approach can be applied to the second moment of  $\tilde{F}(t)$  the estimator of  $f(t)$ , in order to obtain its variance. The example given in this section is simple enough to derive a symbolic expression of the variance. It states that:

$$\text{Var}(\tilde{F}(t)) = \frac{\alpha f_0 t}{\frac{\hat{\nu}}{\alpha f_0} + \left(\frac{\hat{\nu}}{\alpha f_0} - 1\right) \alpha f_0 t} f(t)^2 \quad (29a)$$

if

$$\hat{\nu} \geq \alpha f_0 \quad \text{or} \quad \left(\frac{\alpha f_0}{\hat{\nu}} - 1\right) \alpha f_0 t < 1 \quad (29b)$$

, otherwise  $\text{Var}(\tilde{F}(t))$  is infinite.

Interestingly, the behaviour of  $\tilde{F}$  varies qualitatively with the quality of  $\hat{\nu}$  as a global bound of the extinction frequency (of which the maximum is  $\alpha f_0$ ):

- If  $\hat{\nu} > \alpha f_0$ , the relative variance of  $\tilde{F}(t)$ , defined as  $\text{Var}(\tilde{F}(t))/f(t)^2$ , tends to a finite value when

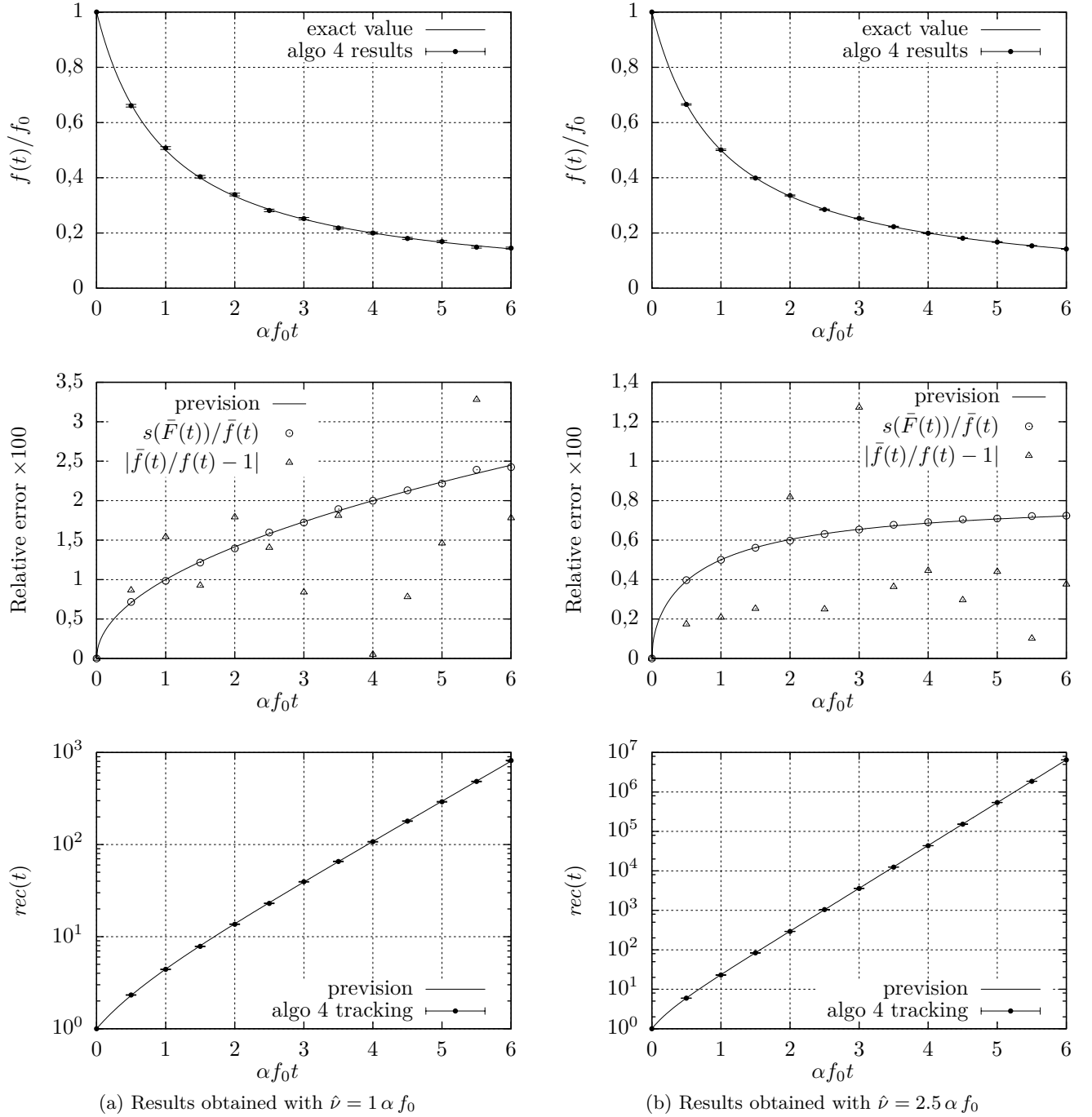


FIG. 7. Results obtained by algorithm 4, solving the Eq. (20).  $f(t)$  was calculated at different  $t$ , using two different values of  $\hat{\nu}$  in columns (a) and (b). The four bottom graphs compare the predictions in Eqs. (28) and (29) with what algorithm 4 has done. Each point was obtained through running  $10^4$  realizations of algorithm 4.

$t \rightarrow +\infty$ . So the absolute variance of  $\tilde{F}(t)$  tends toward 0 while  $t \rightarrow +\infty$ .  $\tilde{F}(t)$  is a usable estimator of  $f(t)$  for every  $t$ .

- If  $\hat{\nu} = \alpha f_0$ , the relative variance of  $\tilde{F}(t)$  grows linearly to infinity with  $t$ ; the absolute variance of  $\tilde{F}(t)$  still tends towards 0 while  $t \rightarrow +\infty$ .  $\tilde{F}(t)$  is thus still a reasonable estimator of  $f(t)$  regardless

of  $t$ .

- If  $\hat{\nu} < \alpha f_0$ , the variance of  $\tilde{F}(t)$  (absolute or relative) reaches infinity for a finite value of the time  $t$ , and for all subsequent times. In these conditions, obtaining the convergence of a Monte-Carlo procedure estimating  $f(t)$  can be very difficult.

e. *Algorithm 4 was actually run* with one aim being to confirm what is affirmed in Eqs. (28) and (29). Some results are given in Fig. 7.

The indications stated above about the recursion and the variance of algorithm 4 are confirmed. Noticeably, we do not have that sharp increase in the estimator variance with simulated time, which is observed in algorithm 2 aimed at solving the BKW mode.

Furthermore, in Fig. 7, as in Eqs. (28) and (29), it can be understood that a compromise needs to be found in the parameter  $\hat{\nu}$ : between a low variance associated with a high recursion, and a low recursion associated with a high variance. This kind of compromise is in fact present when designing recursive MC algorithms solving any problem presented in this paper. For example, with oversampling strategies we have been able to increase simulatable physical times in the BKW mode of the previous section by several mean free flight times. This will be the subject of a future work.

#### IV. EXAMPLE: HARMONIC TRAP

a. *In this section we solve* the Boltzmann equation with the MCM, in a second academic case where a symbolic solution is available. In this case, the gas is no longer uniform, and forms a cloud around the origin which swells and contracts periodically. Compared to the BKW mode, we have now to account for the ballistic transport and for a variable collision frequency.

The physical case under consideration here is nevertheless very particular, because it belongs to the kernel of the collision operator – *ie* collisions have no influence –, although it is not the barometric equilibrium. This possibility has been known since the works of Boltzmann himself [48], and has been revisited recently in the field of cold atom gas manipulation [41].

We chose our precise test case in the collision operator kernel, built as simply as possible:

- The molecules are subjected to a constant and purely harmonic force calling them back to the origin. This force subjects the particles to an acceleration:

$$\vec{a} \equiv \vec{a}(\vec{r}) = -\omega^2 \vec{r} \quad (30)$$

where  $\vec{r}$  is the position.

- The gas has no global kinetic moment around the origin.

Knowing this, the equilibrium distributions constitute a set parametrized by two quantities, like the total amount of matter  $n$  and the thermal RMS speed on each axis  $c_q$ . In this case of elastic confinement, the collision operator kernel extends to breathing modes oscillating at twice the trap frequency, with two additional parameters, such as  $\Delta c_q^2$  the amplitude of the thermal energy oscillations and  $\phi_0$  a phase at the origin of time. In these breathing

modes, the distribution of molecules is always and everywhere Maxwellian, with density, peculiar speed, and thermal energy:

$$\eta_{\text{cok}}(\vec{r}; t) = n p_{\mathcal{N}\left(\vec{0}; \frac{(1+\epsilon \sin \phi(t)) c_{q, \text{eq}}^2}{\omega^2} \bar{I}\right)}(\vec{r}) \quad (31a)$$

$$\vec{v}_{\text{cok}}(\vec{r}; t) = \frac{\epsilon \cos \phi(t)}{1 + \epsilon \sin \phi(t)} \omega \vec{r} \quad (31b)$$

$$c_{q, \text{cok}}(t)^2 = \frac{(1 - \epsilon^2) c_{q, \text{eq}}^2}{1 + \epsilon \sin \phi(t)} \quad (31c)$$

where  $\phi(t)$  stands for  $2\omega t + \phi_0$ ,  $c_{q, \text{eq}}$  is the thermal speed in the equilibrium distribution with same total mass and same total mechanical energy,  $\epsilon$  equals  $\frac{\Delta c_q^2}{c_{q, \text{eq}}^2}$ , and  $p_{\mathcal{N}(\vec{0}; \bar{V})}$  denotes the density of the centred multidimensional normal probability law with covariance matrix  $\bar{V}$ . The resulting physical example is presented in Fig. 8.

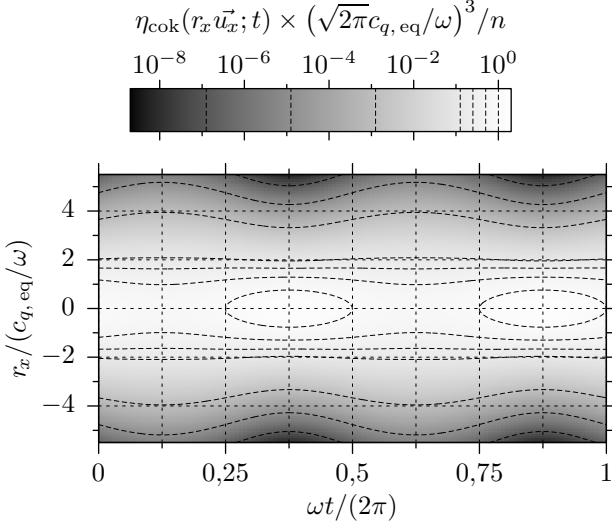
Because we do not want to have only ballistic dynamics, we need to choose a collision model. For the sake of simplicity, we chose the isotropic Maxwell collision model: the differential collision cross-section  $\sigma_F = \kappa/(4\pi g)$  where  $g$  is the relative velocity of particles and  $\kappa$  is a constant.

b. *Introducing null-collisions*, the Boltzmann equation can be written in our case:

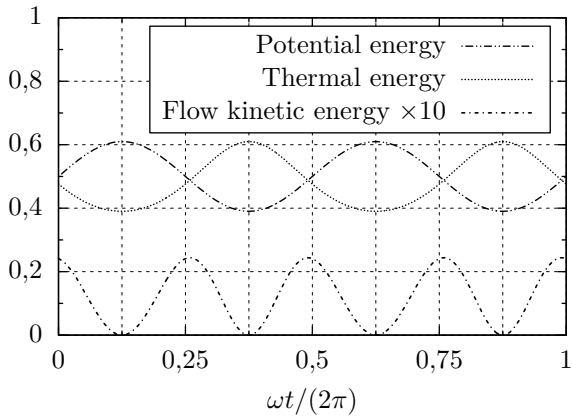
$$\begin{aligned} \partial_t f(\vec{r}; \vec{c}; t) + \vec{c} \cdot \vec{\nabla}_{\vec{r}} f(\vec{r}; \vec{c}; t) - \omega^2 \vec{r} \cdot \vec{\nabla}_{\vec{c}} f(\vec{r}; \vec{c}; t) = \\ -\hat{\nu}(\vec{r}; \vec{c}; t) f(\vec{r}; \vec{c}; t) \\ + \left( \hat{\nu}(\vec{r}; \vec{c}; t) - \kappa \int_{E_c} d\vec{c}_* f(\vec{r}; \vec{c}_*; t) \right) f(\vec{r}; \vec{c}; t) \\ + \kappa \int_{E_c} d\vec{c}_* \int_{E_u} \frac{d\vec{u}}{4\pi} f(\vec{r}; \vec{c}'; t) f(\vec{r}; \vec{c}_*'; t) \quad (32) \end{aligned}$$

where  $\vec{c}'$  and  $\vec{c}_*'$  are given in Eq. (6), and  $\hat{\nu}$  is an arbitrary raised collision frequency. Considering that the distribution is known at  $t = 0$  (as in section II), and using Liouville's theorem, Eq. (32) can be turned into a Fredholm counterpart:

$$\begin{aligned} f(\vec{r}; \vec{c}; t) = \int_{-\infty}^t dt' \hat{\nu}(\vec{r}_b(t'); \vec{c}_b(t'); t') \times \\ \exp \left( - \int_{t'}^t dt'' \hat{\nu}(\vec{r}_b(t''); \vec{c}_b(t''); t'') \right) \times \\ \left( H(-t') f(\vec{r}_b(0); \vec{c}_b(0); 0) + H(t') \times \right. \\ \left. \left( \left( 1 - \frac{\nu_t(\vec{r}_b(t'); \vec{c}_b(t'); t')}{\hat{\nu}(\vec{r}_b(t'); \vec{c}_b(t'); t')} \right) f(\vec{r}_b(t'); \vec{c}_b(t'); t') + \right. \right. \right. \\ \left. \left. \left. \frac{s_{is}(\vec{r}_b(t'); \vec{c}_b(t'); t')}{\hat{\nu}(\vec{r}_b(t'); \vec{c}_b(t'); t')} \right) \right) \right) \quad (33a) \end{aligned}$$



(a) Density of matter along the  $(Ox)$  axis of the ordinary space, as a function of the time. The physical situation has spherical symmetry. The dashed lines are density level sets, spaced with a factor 2 or a factor 100.



(b) Distribution of the total mechanical energy of the gas, as a function of the time.

FIG. 8. Presentation of the physical situation of the harmonic trap described in Eq. (31). The parameters  $\epsilon = \frac{9}{41}$  and  $\phi_0 = 0$  are chosen, as in section V.

with  $\vec{r}_b$  and  $\vec{c}_b$  describing the ballistic trajectory flowing past  $(\vec{r}; \vec{c})$  at  $t$ :

$$\begin{cases} \partial_{t'} \vec{r}_b(t') = \vec{c}_b(t') \\ \partial_{t'} \vec{c}_b(t') = -\omega^2 \vec{r}_b(t') \end{cases} \quad \text{with the IC} \quad \begin{cases} \vec{r}_b(t) = \vec{r} \\ \vec{c}_b(t) = \vec{c} \end{cases} \quad (33b)$$

and  $\nu_t$  and  $s_{is}$  are the real extinction and source term:

$$\nu_t(\vec{r}; \vec{c}; t) = \kappa \int_{E_c} d\vec{c}_* f(\vec{r}; \vec{c}_*; t) \quad (33c)$$

$$s_{is}(\vec{r}; \vec{c}; t) = \kappa \int_{E_c} d\vec{c}_* \int_{E_u} \frac{d\vec{u}'}{4\pi} f(\vec{r}; \vec{c}'; t) f(\vec{r}; \vec{c}_*'; t) \quad (33d)$$

The raised extinction frequency  $\hat{\nu}$  can be used as a

sampling guide for  $t'$ . Then, by choosing probability densities in order to sample  $\vec{c}_*$  and  $\vec{u}'$ , Eq. (33) can be converted into Monte-Carlo algorithm 5, intended to estimate  $f(\vec{r}; \vec{c}; t)$  with  $(\vec{r}; \vec{c}; t) \in E_r \times E_c \times \mathbb{R}^+$  – where  $E_r$  denotes the space of positions.

Algorithm 5 has an amazing feature: if the initial distribution is in the kernel of the collision operator – as described in Eq. (31) –, then whatever the choices retained for  $\hat{\nu}$ ,  $\vec{C}_*$ , and  $\vec{U}'$ , the result of algorithm 5 has a null variance. To our knowledge, this is the first Monte-Carlo algorithm which exhibits a zero variance result independently of the sampling choices[49].

*Principle of proof (Null variance of algorithm 5).* We call  $\tilde{F}(\vec{r}; \vec{c}; t)$  an estimator of  $f(\vec{r}; \vec{c}; t)$ , obtained through algorithm 5. We assume that the initial distribution  $f(\vec{r}; \vec{c}; t = 0)$  is everywhere Maxwellian, with the first moments described in Eq. (31).

An essential lemma for this proof is the following: for any arbitrary choice of  $(\vec{r}; \vec{c}; t; t') \in E_r \times E_c \times \mathbb{R} \times \mathbb{R}$ , a density value at  $(\vec{r}; \vec{c}; t)$  is compatible with a Maxwellian distribution of which the first moments are described in Eq. (31), if and only if the same density value at  $(\vec{r}_b(t'); \vec{c}_b(t'); t')$  is compatible with a Maxwellian distribution of which the first moments are described in Eq. (31) with substitution of  $t$  by  $t'$ . This means, by virtue of Liouville's theorem, that an oscillating Maxwellian distribution, as described in Eq. (31), is compatible with the ballistic transport in the given force field. The proof of this, and its extension to more general expressions of the collision operator kernel, can be found in [41] and will not be repeated here.

Now consider the following induction hypothesis, to apply anywhere in an estimation tree:  $\tilde{F}(\vec{r}; \vec{c}; t)$  equals with no variance  $f(\vec{r}; \vec{c}; t)$ , which describes a Maxwellian distribution, the first moments of which are given in Eq. (31).

Starting algorithm 5, there are two possibilities:  $T' \leq 0$  and we are at a leaf of the estimation tree, or  $T' > 0$  and we are at a non-leaf node of the tree.

If  $T' \leq 0$  then:

$$\tilde{F}(\vec{r}; \vec{c}; t) = f(\vec{r}_b(0); \vec{c}_b(0); 0) \quad (34)$$

Because of the initial condition and of the lemma, the induction hypothesis is valid.

If  $T' > 0$  then:

$$\begin{aligned} \tilde{F}(\vec{r}; \vec{c}; t) = & \tilde{F}_1(\vec{r}_b(T'); \vec{c}_b(T'); T') + \\ & \frac{\kappa}{4\pi p_{\vec{C}_*}(\vec{C}_*) p_{\vec{U}'}(\vec{U}') \hat{\nu}(\vec{r}_b(T'); \vec{c}_b(T'); T')} \times \\ & \left( \tilde{F}_3(\vec{r}_b(T'); \vec{C}'; T') \tilde{F}_4(\vec{r}_b(T'); \vec{C}_*'; T') - \right. \\ & \left. \tilde{F}_1(\vec{r}_b(T'); \vec{c}_b(T'); T') \tilde{F}_2(\vec{r}_b(T'); \vec{C}_*'; T') \right) \end{aligned}$$

where  $\vec{C}'$  and  $\vec{C}_*'$  are the RVs corresponding to the values  $\vec{c}'$  and  $\vec{c}_*'$  in algorithm 5. If the induction hypothesis

```

Input: A point  $(\vec{r}; \vec{c}; t)$  in  $E_r \times E_c \times \mathbb{R}^+$ 
Output: A point estimate of  $f(\vec{r}; \vec{c}; t)$ 

Sample  $T'$  in  $(-\infty; t]$ , with the density  $p_{T'} : t' \mapsto \hat{\nu}(\vec{r}_b(t'); \vec{c}_b(t'); t') \exp(-\int_{t'}^t dt'' \hat{\nu}(\vec{r}_b(t''); \vec{c}_b(t''); t''))$ :  $t'$  is obtained;
if  $t' \leq 0$  then
  return  $f(\vec{r}_b(0); \vec{c}_b(0); 0)$ ;
else
  Sample  $\vec{C}_*$ :  $\vec{c}_*$  is obtained;
  Sample  $\vec{U}'$ :  $\vec{u}'$  is obtained;
   $\vec{c}' \leftarrow \frac{1}{2}(\vec{c}_b(t') + \vec{c}_* + \|\vec{c}_b(t') - \vec{c}_*\| \vec{u}')$ ;
   $\vec{c}'_* \leftarrow \frac{1}{2}(\vec{c}_b(t') + \vec{c}_* - \|\vec{c}_b(t') - \vec{c}_*\| \vec{u}')$ ;
  Estimate  $f(\vec{r}_b(t'); \vec{c}_b(t'); t')$  using this algorithm:  $\tilde{f}_1(\vec{r}_b(t'); \vec{c}_b(t'); t')$  is obtained;
  Estimate  $f(\vec{r}_b(t'); \vec{c}_*; t')$  using this algorithm:  $\tilde{f}_2(\vec{r}_b(t'); \vec{c}_*; t')$  is obtained; // independently of  $\tilde{f}_1(\vec{r}_b(t'); \vec{c}_b(t'); t')$ 
  Estimate  $f(\vec{r}_b(t'); \vec{c}'; t')$  using this algorithm:  $\tilde{f}_3(\vec{r}_b(t'); \vec{c}'; t')$  is obtained;
  Estimate  $f(\vec{r}_b(t'); \vec{c}'_*; t')$  using this algorithm:  $\tilde{f}_4(\vec{r}_b(t'); \vec{c}'_*; t')$  is obtained; // independently of  $\tilde{f}_3(\vec{r}_b(t'); \vec{c}'; t')$ 
  return  $\tilde{f}_1(\vec{r}_b(t'); \vec{c}_b(t'); t') + \kappa \frac{\tilde{f}_3(\vec{r}_b(t'); \vec{c}'; t') \tilde{f}_4(\vec{r}_b(t'); \vec{c}'_*; t') - \tilde{f}_1(\vec{r}_b(t'); \vec{c}_b(t'); t') \tilde{f}_2(\vec{r}_b(t'); \vec{c}_*; t')}{4\pi p_{\vec{C}_*}(\vec{c}_*) p_{\vec{U}'}(\vec{u}') \hat{\nu}(\vec{r}_b(t'); \vec{c}_b(t'); t')}$ ;

```

**Algorithm 5:** Algorithm for estimating  $f(\vec{r}; \vec{c}; t)$ , valid in the conditions of the harmonic trap described in sections IV and V

holds for  $\tilde{F}_1$ ,  $\tilde{F}_2$ ,  $\tilde{F}_3$  and  $\tilde{F}_4$ , then:

$$\begin{aligned} \tilde{F}(\vec{r}; \vec{c}; t) &= f(\vec{r}_b(T'); \vec{c}_b(T'); T') + \\ &\quad \frac{\kappa}{4\pi p_{\vec{C}_*}(\vec{C}_*) p_{\vec{U}'}(\vec{U}') \hat{\nu}(\vec{r}_b(T'); \vec{c}_b(T'); T')} \times \\ &\quad \left( f(\vec{r}_b(T'); \vec{C}'; T') f(\vec{r}_b(T'); \vec{C}'_*; T') - \right. \\ &\quad \left. f(\vec{r}_b(T'); \vec{c}_b(T'); T') f(\vec{r}_b(T'); \vec{C}_*; T') \right) \end{aligned}$$

Considering now that  $f$  at  $(\vec{r}_b(T'); T')$  follows a Maxwellian distribution, which respects the detailed balance, we conclude that:

$$\tilde{F}(\vec{r}; \vec{c}; t) = f(\vec{r}_b(T'); \vec{c}_b(T'); T') \quad (35)$$

Following the lemma, the induction hypothesis is valid.

As long as the estimation tree is finite (which brings conditions on  $\hat{\nu}$ ), the induction hypothesis applies from the leaves of the tree to any node of the tree, root included.  $\square$

Some numerical experiments (not displayed here) have confirmed this result.

## V. EXAMPLE: HARMONIC TRAP WITHOUT LOCAL EQUILIBRIUM

a. *There is not a lot to illustrate* in the previous section: in the physical case described, the proposed algorithm has zero variance. There are of course a lot of possible modifications of algorithm 5 which break with this state of affairs. We have however chosen to modify the physical case under study, as it seemed pointless to

present a new algorithm, with the only noticeable characteristic being less efficient than the previous one.

The physical case of this section is a mix between the case of the previous section and the BKW mode. We suppose the same external force field, and the same first moments at the initial time, as in section IV. But now, at the initial condition, at each point of space the distribution of speeds is the BKW mode distribution at maximal disequilibrium. This means that at every point of space the initial distribution of speeds is the one described in Eq. (18), translated and scaled to accord with the density, peculiar speed, and temperature prescribed at initial time  $t = 0$  by Eq. (31).

After the initial condition, the system will evolve in a different way to that explained in section IV. The differences appear even in macroscopic quantities. As far as the authors know, there is today no symbolic description available of the evolution of our system. Nevertheless, two limiting situations are easily described:

- If the cross-sections are null (ie there are no collisions), the evolution of the system is made only by ballistic transport. This is symbolically calculable, in a harmonic force field.
- If the cross-sections are not null, the final state of the gas is exactly the oscillating state described in the previous section IV, in Eq. (31). This can be demonstrated using the collisional invariants existing in our system. Considering these, the only state belonging to the collision operator kernel that the system can reach is the one described in Eq. (31).

b. *In order to build simulations*, the last remaining parameters must be set.

We chose  $\epsilon = \frac{9}{41}$  and  $\phi_0 = 0$ , and this set the initial condition. The other parameters  $\omega$ ,  $n$ , and

```

Input: A point  $(\vec{r}; \vec{c}; t)$  in  $E_r \times E_c \times \mathbb{R}^+$ 
Output: A point estimate of  $f(\vec{r}; \vec{c}; t)$ 

 $t' \leftarrow t;$ 
repeat
  Sample  $T^\diamond$  in  $(-\infty; t']$  following an exponential law to the left of  $t'$ , with constant  $\hat{\nu}$ :  $t^\diamond$  is obtained;
  if  $t^\diamond \leq 0$  then
    return  $f(\vec{r}_b(0); \vec{c}_b(0); 0)$ ;
  Calculate  $\eta_{\text{cok}}(\vec{r}_b(t^\diamond); t^\diamond)$ ;  $\eta^\diamond$  is obtained;
   $\hat{\nu}' \leftarrow \frac{1}{e} \left( \frac{5}{3} \right)^{\frac{5}{2}} \kappa \eta^\diamond$ ;
   $t' \leftarrow t^\diamond$ ;
  Sample  $R$  following a uniform standard law;  $r$  is obtained;
until  $r\hat{\nu} < \hat{\nu}'$ ;
Calculate  $c_{q, \text{cok}}(t')$ ;  $c_q'$  is obtained;
Calculate  $\vec{v}_{\text{cok}}(\vec{r}_b(t'); t')$ ;  $\vec{v}'$  is obtained;
Sample  $\vec{C}_*$  following a Maxwellian distribution, with peculiar speed  $\vec{v}'$  and RMS speed  $c_q'$ :  $\vec{c}_*$  is obtained;
Sample  $\vec{U}'$  isotropically:  $\vec{u}'$  is obtained;
 $\vec{c}' \leftarrow \frac{1}{2} (\vec{c}_b(t') + \vec{c}_* + \|\vec{c}_b(t') - \vec{c}_*\| \vec{u}')$ ;
 $\vec{c}'_* \leftarrow \frac{1}{2} (\vec{c}_b(t') + \vec{c}_* - \|\vec{c}_b(t') - \vec{c}_*\| \vec{u}')$ ;
Estimate  $f(\vec{r}_b(t'); \vec{c}_b(t'); t')$  using this algorithm:  $\tilde{f}_1(\vec{r}_b(t'); \vec{c}_b(t'); t')$  is obtained;
Estimate  $f(\vec{r}_b(t'); \vec{c}_*; t')$  using this algorithm:  $\tilde{f}_2(\vec{r}_b(t'); \vec{c}_*; t')$  is obtained; // independently of  $\tilde{f}_1(\vec{r}_b(t'); \vec{c}_b(t'); t')$ 
Estimate  $f(\vec{r}_b(t'); \vec{c}'; t')$  using this algorithm:  $\tilde{f}_3(\vec{r}_b(t'); \vec{c}'; t')$  is obtained;
Estimate  $f(\vec{r}_b(t'); \vec{c}'_*; t')$  using this algorithm:  $\tilde{f}_4(\vec{r}_b(t'); \vec{c}'_*; t')$  is obtained; // independently of  $\tilde{f}_3(\vec{r}_b(t'); \vec{c}'; t')$ 
return  $\tilde{f}_1(\vec{r}_b(t'); \vec{c}_b(t'); t') + \frac{\kappa (\sqrt{2\pi} c_q')^3}{\hat{\nu}'} \exp\left(\frac{(\vec{c}_* - \vec{v}')^2}{2 c_q'^2}\right) \left( \tilde{f}_3(\vec{r}_b(t'); \vec{c}'; t') \tilde{f}_4(\vec{r}_b(t'); \vec{c}'_*; t') - \tilde{f}_1(\vec{r}_b(t'); \vec{c}_b(t'); t') \tilde{f}_2(\vec{r}_b(t'); \vec{c}_*; t') \right)$ ;

```

**Algorithm 6:** Algorithm for estimating  $f(\vec{r}; \vec{c}; t)$ , valid in the conditions of the harmonic trap described in sections IV and V. The sampling choices detailed in section V are used.

$c_{q, \text{eq}}$  are irrelevant since they are squeezed during non-dimensionalization. This is the choice we made while expounding the physical case of section IV in Fig. 8. We must also specify the collision model: we chose  $\kappa$  such as  $\frac{n \kappa \omega^2}{c_{q, \text{eq}}^3} = 3$ .

Finally, we need to specify  $\hat{\nu}$ ,  $\vec{C}_*$ , and  $\vec{U}'$ .  $\vec{U}'$  will follow an isotropic law, as in section II.  $\vec{C}_*$  is set to a Maxwellian sampling; the Maxwellian bell is adjusted according to the final distribution, *ie* it is centred on  $\vec{v}_{\text{cok}}(\vec{r}; t')$  and reduced to  $c_{q, \text{cok}}(t')$  standard deviation given in Eq. (31), where  $t'$  is the collision date. As we wanted  $\hat{\nu}$  as a credible bound of the collision frequency, we made the following choice:

$$\hat{\nu} \equiv \hat{\nu}(\vec{r}; t) = \frac{1}{e} \left( \frac{5}{3} \right)^{\frac{5}{2}} \kappa \eta_{\text{cok}}(\vec{r}; t) \quad (36)$$

The pre-factor  $\frac{1}{e} \left( \frac{5}{3} \right)^{\frac{5}{2}}$  is the maximal ratio between the BKW mode initial distribution and the equilibrium distribution with the same first moments. Indeed:

$$\frac{1}{e} \left( \frac{5}{3} \right)^{\frac{5}{2}} = \max_{\vec{c} \in E_c} \frac{f_{\text{BKW}}(\vec{c}; 0)}{(\sqrt{2\pi} c_q)^{-3} \exp(-\vec{c}^2/(2 c_q^2))} \quad (37)$$

where  $f_{\text{BKW}}(\vec{c}; 0)$  is given by Eq. (18).

Sampling a collision date  $t'$  using the raised collision frequency  $\hat{\nu}$  given in Eq. (36) can be tricky: we need to apply the Beer extinction law to the gas density described in Eq. (31), along an elliptic ballistic trajectory... To

achieve this, we use  $\hat{\nu}$  as the true extinction in an internal Null Collision Algorithm. This NCA uses as a raised collision frequency the global maximum of  $\hat{\nu}$  defined in Eq. (36), reached in the centre of the gas cloud at its maximum contraction. We denote it  $\hat{\nu}$ , and it equals:

$$\hat{\nu} = \frac{1}{e} \left( \frac{5}{3} \right)^{\frac{5}{2}} \kappa \eta_{\text{cok}}(\vec{0}; t) \Big|_{\sin \phi(t) = -1} \quad (38)$$

$$= \frac{1}{e} \left( \frac{5}{3} \right)^{\frac{5}{2}} \kappa n \left( \frac{\omega}{\sqrt{2\pi} \sqrt{1 - \epsilon} c_{q, \text{eq}}} \right)^3 \quad (39)$$

With all these choices, algorithm 5 becomes algorithm 6.

c. We then ran algorithm 6 with all the physical and numerical settings stated previously in this section. The results are displayed in Figs. 9 and 10. What is noted on these figures as *rec* is the mean recursion of algorithm 6, which means the mean number of internal calls of algorithm 6 as it is written, when calling it to estimate  $f$  at a particular point  $(\vec{r}; \vec{c}; t)$  of the phase space-time.

In Fig. 9 the distribution function  $f$  is followed at two constant probe points of the phase space. As in the previous sections, all calculated points are independent, which is why we can focus on any particular region of the phase space-time, as we did around  $\omega t = 3$ .

Fig. 10 shows the distribution of the mass along the potential energy (or equivalently, along the distance about the origin). The fraction of the mass more distant from

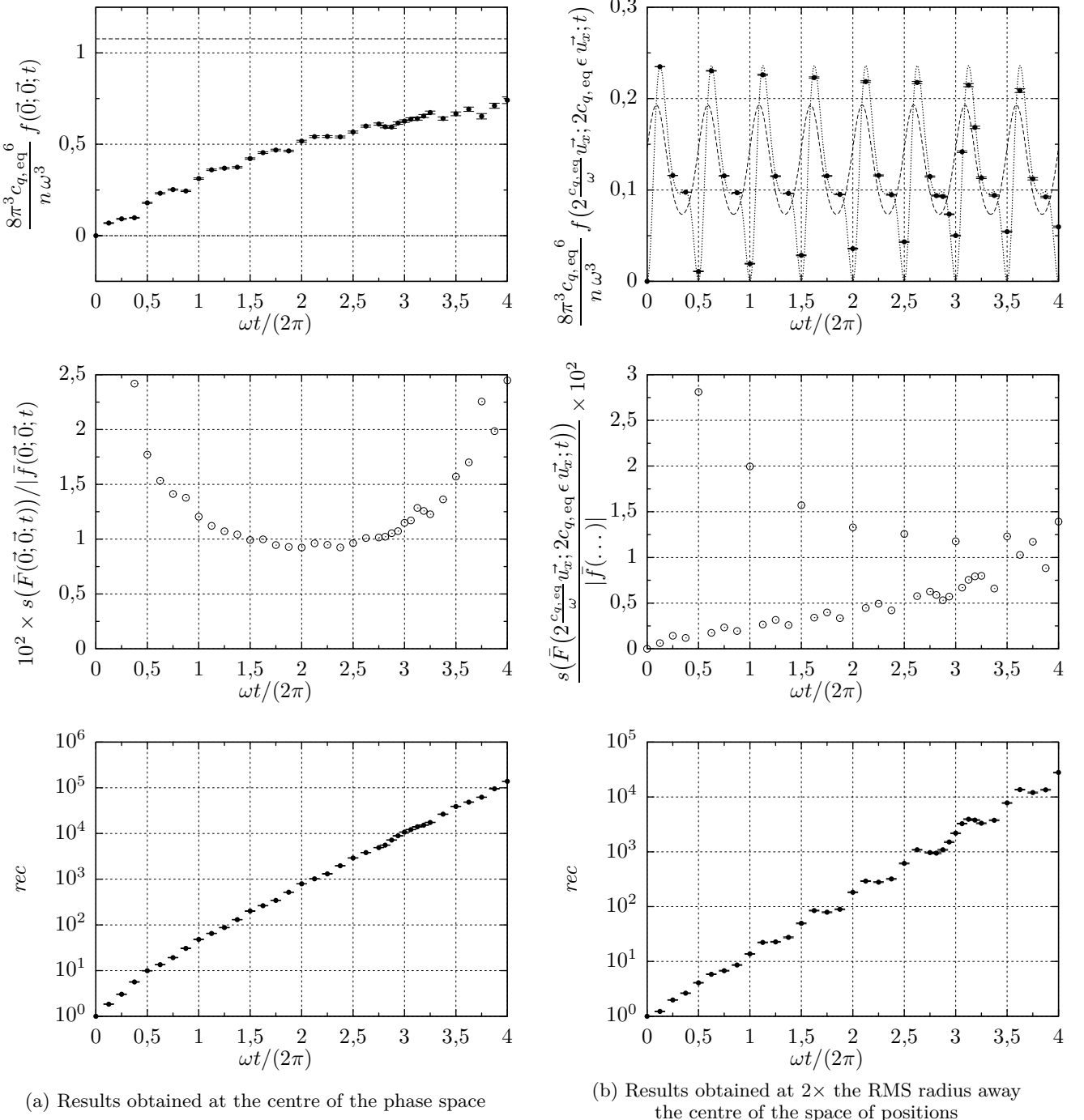


FIG. 9. Results obtained by algorithm 6, with the choices presented in subsection V 0 b, and applied to the harmonic trap problem described in section IV and V. Two probe points in the phase space are considered, where we follow the distribution function  $f$  along the time  $t$ . These probe points  $(\vec{r}; \vec{c})$  comply with the constraint  $\vec{c} = \vec{v}_{\text{cok}}(\vec{r}; 0)$ , such that there  $f = 0$  at the initial instant. The graphs on the top give a graphical comparison between the results (given with confidence intervals of 1 standard deviation), the values predicted in the final oscillating state (dashed lines), and the values predicted by ballistic transport of the initial condition (dotted lines). The graphs of the middle line show, with the same results, the relative standard deviation given by the calculation. The graphs of the bottom display the mean recursivity of algorithm 6 computing the points on the graphs above. Each displayed points has been obtained through running  $10^4$  realizations of algorithm 6.

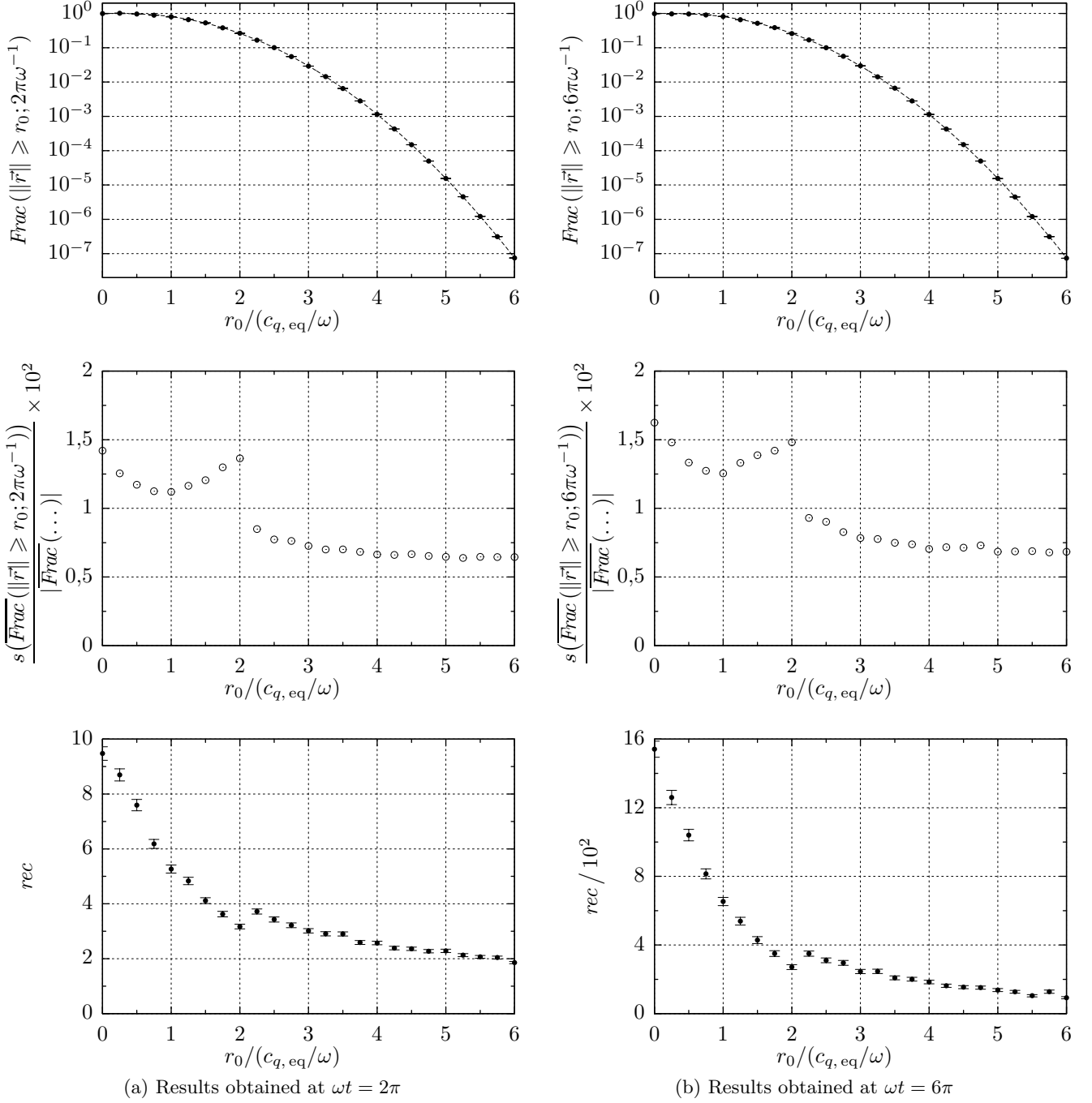


FIG. 10. Results obtained by algorithm 7 combined with the sampling laws listed in Eq. (40) and section V 0 b, and applied to the harmonic trap problem described in sections IV and V. We calculate the distribution of particles along the radius  $\|\vec{r}\|$ , *i.e.* how many particles are more distant from the origin than any given threshold  $r_0$ ; only two dates are considered. The graphs at the top give a graphical comparison between the results (given with confidence intervals of 1 standard deviation), and the values predicted in the final oscillating state (dashed lines) (ballistic transport of the initial condition leads to the same results, in these precise cases). The graphs in the middle line show, with the same results, the relative standard deviation given by the calculation. The graphs at the bottom display the mean recursivity of algorithm 6 called by algorithm 7, when computing the points on the graphs above. Each displayed point was obtained through running  $10^4$  realizations of algorithm 7.

the origin than a fixed threshold  $r_0$  is computed, as a function of this threshold. This is an integral of the distribution function  $f$  over the phase space. It is calculated using algorithm 6, with an additional initial sampling of a radius  $\vec{r}_f$  and a velocity  $\vec{c}_f$ . The result is algorithm 7. The sampling law of  $(\vec{R}_f; \vec{C}_f)$  is similar to the one given in Eq. (19), indeed:

$$\left\{ \begin{array}{l} \vec{R}_f = R_f \vec{U}_f \quad \text{with} \\ p_{R_f}(r_f) = \begin{cases} \frac{r_0 \left( \left( \frac{\omega r_0}{c_{q, \text{eq}}} \right)^2 - 2 \right)}{\left( \left( \frac{\omega r_0}{c_{q, \text{eq}}} \right)^2 - 2 \right) (r_f - r_0) + r_0} & \text{if } \omega r_0 > 2c_{q, \text{eq}} \\ \frac{2c_{q, \text{eq}}/\omega}{(2c_{q, \text{eq}}/\omega + r_f - r_0)^2} & \text{if } \omega r_0 \leq 2c_{q, \text{eq}} \end{cases} \\ p_{\vec{U}_f}(\vec{u}_f) = (4\pi)^{-1} \\ \vec{C}_f \text{ of law } \mathcal{N} \left( \vec{v}_{\text{cok}}(\vec{R}_f; t); c_{q, \text{cok}}(t)^2 \bar{\bar{I}} \right) \end{array} \right. \quad (40)$$

**Input:** A radius  $r_0$  and a time  $t$

**Output:** A point estimate of  $\text{Frac}(\|\vec{r}\| \geq r_0; t)$ , the fraction of particles more distant than  $r_0$  from the origin at time  $t$

Sample  $R_f$ :  $r_f$  is obtained;  $\quad // \quad r_f \geq r_0$   
 Sample  $\vec{U}_f$ :  $\vec{u}_f$  is obtained;  
 Sample  $\vec{C}_f$ :  $\vec{c}_f$  is obtained;  
 Estimate  $f(r_f \vec{u}_f; \vec{c}_f; t)$  using algorithm 6:  $\tilde{f}(r_f \vec{u}_f; \vec{c}_f; t)$  is obtained;  
**return**  $\frac{r_f^2 \tilde{f}(r_f \vec{u}_f; \vec{c}_f; t)}{p_{R_f}(r_f) p_{\vec{U}_f}(\vec{u}_f) p_{\vec{C}_f}(\vec{c}_f)}$ ;

**Algorithm 7:** Algorithm for estimating fractions of particles with high potential energy, valid in the conditions of the harmonic trap described in sections IV and V

We observe the same behaviours in algorithm 6 as in algorithm 2. The variance of the obtained estimator of  $f$  increases with the simulated physical time. It is however practically insensitive to rarefaction; we can evaluate without difficulty fractions of the mass as small as one millionth.

There is a noticeable decrease in the recursivity of algorithm 6 when the probe points move away from the origin. This was an expected result, as the raised collision frequency  $\hat{\nu}$  is higher near the origin. Also, we can appreciate now the usefulness of our somewhat complex raised extinction frequency field  $\hat{\nu}$  set in Eq. (36). If we had instead used a constant raised collision frequency such as  $\hat{\nu}$  defined in Eq. (38), the mean recursion would have been higher than shown in Figs. 9 and 10. However, it is already very high there, especially considering that at the maximum physical time we probed, the system was still very far from its final state.

## VI. CONCLUSION AND PERSPECTIVES

*a.* We have numerically solved the Boltzmann equation of gas kinetics in several test cases, using the Monte-Carlo method. It is the ordinary Monte-Carlo method, as used in linear physics, without bias, and where particle paths are computed independently. The algorithms that we have proposed are based on a second kind Fredholm writing of the Boltzmann equation, and rely on the following of virtual particles from their arrivals to their sources. As far as the authors know, this is the first numerical method in gas kinetics which thus travels along time, backwards.

This building of particle paths, from the end to the start, brings an interesting property to the method. No difficulty appears when focusing on low crowded parts of the phase space. For the same reason we can carry out *probe calculus*. This ability is widely known in linear transport physics. An example from radiative transfer is the prediction of the view of a satellite looking at the Earth: it is commonly known that one can calculate the image by sampling rays built as incoming to the satellite and directed from the Earth, and then by evaluating the possible sources of these rays; and that it is unnecessary to start by computing the whole irradiance field around the Earth. The paths built from their destination can explore the phase space, and catch the information strictly necessary to compute the desired result.

*b.* This possibility to use particle paths built toward sources is usually considered to be linked to a propagative insight of the phenomenon. This means that what is observed at the probe point is a sum of the contributions of all possible paths coming from sources. This insight remains part of our approach, and the non-linearity is taken into account at the nodes of the henceforth branching paths. So the contributing paths are now contributing trees. Each tree consists of the path of the incoming particle, plus the paths of its collision partners, plus the paths of the collision partners of the aforementioned partners, *etc...* We have obtained an arborescent propagation.

This comes at a price. When the mean number of collisions encountered by the particles inside the simulated space-time increases, the contributing trees are padded, and the recursivity and estimation variance of our algorithms can make their calculations unaffordable.

We are convinced that this extension of a propagative and statistical point of view, performed here to examine gas kinetics, is amenable to aspects of other non-linear physics problems. Indeed, it has already been applied recently to some of them [12, 14, 16].

*c.* Another striking feature of the computations we have done is the complete absence of any mesh within. This is again a common property of the Monte-Carlo method in linear transport physics, but is new in gas kinetics numericals. Here it is pointless to worry about the good coverage of the space of speeds, about the bias that the mesh introduces, or about the memory usage of

the numerical programme.

If a geometry is present (a possibility not illustrated in this article), it enters the integral formulation of the Boltzmann equation only through an intersection calculus, between surfaces and ballistic trajectories. Otherwise, the boundary conditions in gas kinetics are generally written as integral expressions of the distribution of the outgoing molecules, directly usable in our Monte-Carlo method. This leads the authors to state that taking into account any geometry will bring no difficulty, given that ballistic trajectories are simple enough – typically, straight lines. If very complex geometries come into play, we will be able to use the expertise of the image synthesis community directly [20].

*d.* Finally, setting aside the theoretical implications this work could have, we have still obtained a numerical method in gas kinetics that is very complementary to what is currently available.

It can compute the high energy fractions in the gas very easily, which is reputed to be a high burden for the DSMC method or for fully discretized methods in gas kinetics. These fractions can be very important from the

applicative point of view, because some processes happen only here – *eg* chemical reactions, ionization events, nuclear reactions or degradation processes.

However, today it works mainly in non-stationary problems, where the initial condition plays a major role. Going to stationary situations is very difficult. On the other hand, stationary problems are reputedly easier for the DSMC or fully discretized methods.

## ACKNOWLEDGEMENTS

This work has been sponsored by the French government research-program “Investissements d’avenir” through the ANR program ANR-2012-IS04-0003-03 DEPART, the Laboratories of Excellence ANR-10-LABX-22-01 SOLSTICE and ANR-10-LABX-16-01 IMobS<sup>3</sup>, the ATS program ALGUE of the IDEX of Toulouse ANR-11-IDEX-02 UNITI, by the Occitanie region, and by the LAPLACE laboratory through a BQR program.

---

- [1] J. R. Howell, *Journal of Heat Transfer* **120**, 547 (1998).
- [2] N. Metropolis and S. Ulam, *Journal of the American Statistical Association* **44**, 335 (1949).
- [3] W. L. Dunn and J. K. Shultis, *Exploring Monte Carlo Methods* (Elsevier, 2012) p. 391.
- [4] I. T. Dimov, *Monte Carlo Methods for Applied Scientists* (2008) p. 308.
- [5] I. Karatzas and S. E. Shreve, *Acta Applicandae Mathematicae*, 2nd ed. (Springer-Verlag, 1991) p. 470.
- [6] R. P. Feynman, A. R. Hibbs, and D. F. Styer, *Quantum mechanics and path integrals* (Dover Publications, 2010) p. 371.
- [7] C. J. Umrigar, J. Toulouse, C. Filippi, S. Sorella, and R. G. Hennig, *Physical Review Letters* **98**, 1 (2007), arXiv:0611094 [cond-mat].
- [8] J. H. Curtiss, *Journal of Mathematics and Physics* **32**, 209 (1954).
- [9] M. H. Kalos and P. A. Whitlock, *Monte carlo methods* (John Wiley & Sons, 2008) p. 203.
- [10] S. M. Ermakov, V. V. Nekrutkin, A. Y. Proshkin, and A. F. Sizova, *Doklady Akademii nauk SSSR* **230**, 261 (1976).
- [11] T. V. Gurov, *Mathematica Balkanica* **6**, 237 (1992).
- [12] I. T. Dimov and T. V. Gurov, *Pliska Studia Mathematica Bulgarica* **13**, 117 (2000).
- [13] A. Rasulov, A. N. Karaivanova, and M. Mascagni, *Monte Carlo Methods and Applications* **10**, 551 (2004).
- [14] A. Rasulov, G. Raimova, and M. Mascagni, *Mathematics and Computers in Simulation* **80**, 1118 (2010).
- [15] G. Raimova, *Communications in Statistics - Simulation and Computation* **45**, 2981 (2016).
- [16] P. Henry-Labordère, X. Tan, and N. Touzi, *Stochastic Processes and their Applications* **124**, 1112 (2014), arXiv:1302.4624.
- [17] J. Dauchet, J.-J. Bezian, S. Blanco, C. Caliot, J. Charon, C. Coustet, M. El Hafi, V. Eymet, O. Farges, V. Forest, R. Fournier, M. Galtier, J. Gautrais, A. Khuong, L. Pelissier, B. Piaud, M. Roger, G. Terrée, and S. Weitz, arXiv (2016), arXiv:1610.02684v1.
- [18] J. Dauchet, *Analyse radiative des photobioréacteurs*, Ph.D. thesis, Université Blaise Pascal - Clermont-Ferrand II (2012).
- [19] O. Farges, *Conception optimale de centrales solaires à concentration : application aux centrales à tour et aux installations « beam down »*, Ph.D. thesis, Institut National Polytechnique de Toulouse - École Nationale Supérieure des Mines d’Albi-Carmaux (2014).
- [20] J. De la Torre, G. Baud, J.-J. Bézian, S. Blanco, C. Caliot, J.-F. Cornet, C. Coustet, J. Dauchet, M. El Hafi, V. Eymet, R. Fournier, J. Gautrais, O. Gourmet, D. Joseph, N. Meilhac, A. Pajot, M. Paulin, P. Perez, B. Piaud, M. Roger, J. Y. Rolland, F. Veynandt, and S. Weitz, *Solar Energy* **103**, 653 (2014).
- [21] J. Dauchet, S. Blanco, J.-F. Cornet, and R. Fournier, *Journal of Quantitative Spectroscopy and Radiative Transfer* **161**, 60 (2015).
- [22] J. Charon, S. Blanco, J.-F. Cornet, J. Dauchet, M. El Hafi, R. Fournier, M. K. Abboud, and S. Weitz, *Journal of Quantitative Spectroscopy and Radiative Transfer* **172**, 3 (2015).
- [23] M. Galtier, S. Blanco, C. Caliot, C. Coustet, J. Dauchet, M. El Hafi, V. Eymet, R. Fournier, J. Gautrais, A. Khuong, B. Piaud, and G. Terrée, *Journal of Quantitative Spectroscopy and Radiative Transfer* **125**, 57 (2013).
- [24] J. Novák, A. Selle, and W. Jarosz, *ACM Transactions on Graphics* **33**, 11 (2014).
- [25] L. Szirmay-Kalos, I. Georgiev, M. Magdics, B. Molnár, and D. Légrády, *Eurographics* **36**, 9 (2017).

- [26] H. D. Rees, Solid State Communications **6**, 643 (1968).
- [27] E. Woodcock, T. Murphy, P. Hemmings, and S. Longworth, in *Applications of Computing Methods to Reactor Problems* (1965).
- [28] J. Spanier, SIAM Journal on Applied Mathematics **14**, 702 (1966).
- [29] W. A. Coleman, Nuclear Science and Engineering **32**, 76 (1968).
- [30] H. R. Skullerud, Journal of Physics D: Applied Physics **1**, 1567 (1968).
- [31] S. Longo, Physica A **313**, 389 (2002).
- [32] G. A. Bird, *Molecular Gas Dynamics and the Direct Simulation of Gas Flows* (Clarendon, 1994).
- [33] G. A. Bird, Computers & Mathematics with Applications **35**, 1 (1998).
- [34] E. S. Oran, C. K. Oh, and B. Z. Cybyk, Annual Review of Fluid ... **30**, 403 (1998).
- [35] A. Murrone and P. Villedieu, AerospaceLab , 1 (2011).
- [36] A. I. Khisamutdinov, Transport Theory and Statistical Physics **33**, 69 (2004).
- [37] S. K. Stefanov, SIAM Journal on Scientific Computing **33**, 677 (2011).
- [38] T. M. M. Homolle and N. G. Hadjiconstantinou, Journal of Computational Physics **226**, 2341 (2007).
- [39] P. Degond, G. Dimarco, and L. Pareschi, International Journal for Numerical Methods in Fluids **67**, 189 (2010).
- [40] E. H. Hauge and E. Præstgaard, Journal of Statistical Physics **24**, 21 (1981).
- [41] D. Guéry-Odelin, J. G. Muga, M. J. Ruiz-Montero, and E. Trizac, Physical Review Letters **112**, 1 (2014).
- [42] A. V. Bobylev, Doklady Akademii nauk SSSR **231**, 571 (1976).
- [43] M. Krook and T. T. Wu, Physical Review Letters **36**, 1107 (1976).
- [44] The BKW mode can be generalized to any dimensionality [50].
- [45] M. Moradi, Z. Ayati, and M. A. Mirzazadeh, International Journal of Applied Mathematics and Computation **5**, 35 (2014).
- [46] J.-P. Boeuf and E. Marode, Journal of Physics D: Applied Physics **15**, 2169 (1982).
- [47] N. Andreucci, in *Lecture Notes in Physics* (1985) p. 291.
- [48] L. Boltzmann, *Wissenschaftliche Abhandlungen*, edited by F. Hasenöhrl (Barth, J. A., Leipzig, 1909).
- [49] One could object that the sampling of  $t'$  is imposed, because it is linked to the raised collision frequency  $\hat{\nu}$ ; but  $\hat{\nu}$  is itself arbitrary.
- [50] M. H. Ernst, Physics Letters **69**, 390 (1979).